CHALMERS
UNIVERSITY OF TECHNOLOGY

Decomposing global warming using Bayesian statistics

Impact of internal climate variability and uncertainty of aerosol emissions on the estimated equilibrium climate sensitivity

Master's thesis in Engineering Mathematics and Computational Science

GUSTAV J. E. LJUNGQVIST

Department of Energy and Environment
CHALMERS UNIVERSITY OF TECHNOLOGY
Gothenburg, Sweden 2015

Master's thesis 2015:05

Decomposing global warming using Bayesian statistics

Impact of internal climate variability and uncertainty of aerosol emissions on the estimated equilibrium climate sensitivity

GUSTAV J. E. LJUNGQVIST

CHALMERS
UNIVERSITY OF TECHNOLOGY

Department of Energy and Environment
Division of Physical Resource Theory
Chalmers University of Technology
Gothenburg, Sweden 2015

Decomposing global warming using Bayesian statistics
Impact of internal climate variability and uncertainty of aerosol emissions on the estimated equilibrium climate sensitivity
GUSTAV J. E. LJUNGQVIST

Supervisor: Daniel Johansson, Department of Energy and Environment
Examiner: Daniel Johansson, Department of Energy and Environment

Master's Thesis 2015:05
Department of Energy and Environment
Division of Physical Resource Theory
Chalmers University of Technology
SE-412 96 Gothenburg
Telephone +46 31 772 1000

Typeset in LaTeX
Gothenburg, Sweden 2015

Decomposing global warming using Bayesian statistics
Impact of internal climate variability and uncertainty of aerosol emissions on the estimated equilibrium climate sensitivity
GUSTAV J. E. LJUNGQVIST
Department of Energy and Environment
Chalmers University of Technology

Abstract

In this thesis an energy balance model and regression with internal climate variability indices are employed to model ocean heat content and global mean surface temperatures. The energy balance model takes radiative forcing as input. The nature of the contribution of anthropogenic aerosol emissions to the radiative forcing is not very well-known, and in previous research its path is usually scaled by some factor. Here the path is allowed to vary, which reflects the historical uncertainty. Parameters are estimated using Markov chain Monte Carlo methods. The results show that the aerosol path flexibility substantially increases the probability of very high values of the equilibrium climate sensitivity (ECS), but marginally decreases the most probable value. The inclusion of long-term internal climate variability in the form of the Atlantic Multidecadal Oscillation (AMO) in the regression does not reduce the average error of the estimated temperature. This indicates that observed historical multidecadal temperature oscillations might be better explained by changes in external forcing than by the AMO. It is also shown that including AMO only affects the estimated ECS to a small extent in most scenarios.

Keywords: Global warming, ENSO, Atlantic multidecadal oscillation, hiatus, aerosols, radiative forcing, climate sensitivity.

Acknowledgements

First and foremost I would like to express my sincere gratitude to my supervisor, Associate Professor Daniel Johansson, for introducing me to this subject and guiding me throughout my work with this thesis. I would also like to thank family and friends for the support and encouragement they have provided during my time at Chalmers. Thanks also goes out to my classmates, especially Johan Havås and Christian Söyland, for great cooperation while conducting projects and studying for exams during the last few years.

Gustav J. E. Ljungqvist, Gothenburg, June 2015

List of acronyms and abbreviations

AMO	Atlantic multidecadal oscillation
AOGCM	Atmosphere-ocean general circulation model
AR	Autoregressive
ARx	IPCC WG1 assessment report x
CMIP5	Coupled model intercomparison project (fifth phase of)
CO_2	Carbon dioxide
EBM	Energy balance model
ECS	Equilibrium climate sensitivity
ENSO	El Niño Southern Oscillation
ESM	Earth system model
GCM	General circulation model
GHG	Greenhouse gas
GMST	Global mean surface temperature
ICV	Internal climate variability
IPCC	Intergovernmental Panel on Climate Change
MAE	Mean absolute error
MCMC	Markov chain Monte Carlo
MSE	Mean squared error
NOAA	National Oceanic and Atmospheric Administration
OHC	Ocean heat content
PDF	Probability density function
PDO	Pacific (inter-)decadal oscillation
RF	Radiative forcing
SST	Sea surface temperature

Contents

List of Figures

List of Tables

1

Introduction

Despite humanity's growing emissions of carbon dioxide and other greenhouse gases (GHGs), the global average temperature has not historically been *strictly* increasing. Even though it has increased with almost one degree Celsius over the last century, oscillations on top of the warming trend have always been present. Through the last ∼100 years, there have been two clear periods of intensive warming (1910-1945 and 1975-2000), and two periods of less warming, or even slight cooling (1945-1975 and 2000-present), as seen in Figure 1.1. The trend over the last 10-17 years[1] has

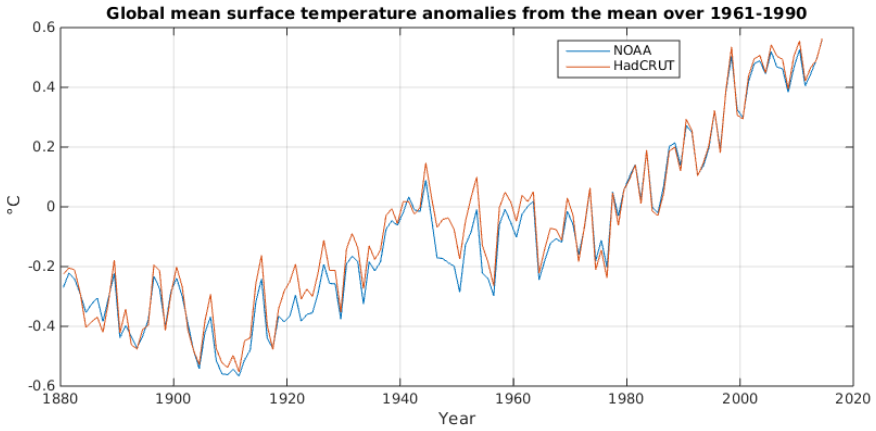

Figure 1.1: Yearly average global mean surface temperatures (GMSTs), 1880 through 2014, from two different datasets.

been labeled "the hiatus", and its reasons have been frequently debated. The atmospheric concentrations of CO_2 and other GHGs have continued to grow unabatedly while the temperature increase has stalled, which has led to a questioning of the widely held view that anthropogenic forcing causes climate warming (Kosaka and Xie, 2013). Since virtually no climate models saw this coming, the hiatus has undermined confidence in climate projections in some groups in society (Watanabe et al., 2014). Climate research is now booming with attempts to explain the apparent interdecadal oscillation in the global mean surface temperature (GMST). Different explanations have different implications on the estimated equilibrium climate sensitivity (ECS), a parameter denoting how many degrees the GMST would rise in the

[1] There is some debate regarding the starting point of the current hiatus. Some see 1998 as the starting year, but it has been argued that this is just the product of cherry-picking the extreme El Niño of 1997/1998, and that the "real" hiatus instead started in 2002 (Cowtan, Jacobs, et al., 2015).

long run given a doubling of the pre-industrial atmospheric CO_2 level. The ECS is hard to quantify from the historical trend due to observational uncertainty, lack of knowledge on the rate of internal variability and large uncertainty in the cooling effect of aerosols. In the IPCC's first working group's fifth assessment report (henceforth IPCC AR5) this parameter was stated to be "likely between 1.5°C and 4.5°C" (Bindoff et al., 2013). This measure is of great importance when attempting to predict what consequences global warming will have for our planet and its inhabitants in the long term. This thesis will investigate how model approximations of the ECS is affected when various sources of internal climate variability are included. It will also attempt to shed further light on the reasons behind interdecadal temperature oscillations, again using different internal climate variability indicators and different assumptions on the cooling induced by aerosols.

All modeling done in this study is focusing on the global scale, and no consideration will be given to regional climate variability. This manifests itself in the assumptions that the surface box is seen as well-mixed over the entire globe, and that the deeper ocean is modeled as a bucket, where temperature only varies with the depth. The climate model considered will be of a simple nature, as more focus is laid on estimating distributions of general scale parameters such as the climate sensitivity, and the impact of internal variability mechanisms.

This thesis is organized as follows. First, an explanation of some internal climate variability mechanisms, as well as a review of previous literature on this subject is given in chapter 2. Some theoretical concepts are explained in chapter 3. The data and the model is described in chapter 4. Results are presented in chapter 5 and discussed in chapter 6. Finally, conclusions are drawn in chapter 7.

2
Background

In this chapter some of the most important internal climate variability mechanisms will be explained. A look at the equilibrium climate sensitivity follows, how it is defined and why it is hard to quantify. Finally a review of previous literature, focusing on similar research questions as this one, is given.

2.1 The El Niño Southern Oscillation

An El Niño is the warm phase of the El Niño Southern Oscillation (ENSO), which is associated with warm temperatures and low pressure in the east-central tropical Pacific. Its opposite, the cool phase, is called La Niña. The strict definition of an El Niño varies, but the definition of Trenberth (1997) is that El Niño is said to occur if 5-month running means of sea surface temperature (SST) anomalies in the NINO3.4 region exceed 0.4°C for 6 months or more. The Niño 3.4 region is defined as the area between 5S-5N and 170-120W, as seen in Figure 2.1. El Niño conditions usually last for 9-12 months, La Niña for 1-3 years, and episodes occur every 2-7 years. (Climate Prediction Center, 2012). Standard conditions for the equatorial Pacific include easterly trade winds transporting warm surface water from the South American coastline towards Australia and Indonesia, and nutrient-rich cold water upwelling in the east. During an El Niño, pressure rises in the west and decreases in the east, weakening or reversing the trade winds. This means that the warm surface water of the Peruvian, Ecuadorian and Colombian coastlines stays where it is, reducing the upwelling of cold water and increasing the sea surface temperature in the area (National Climatic Data Center, 2015a). The warmer surface water releases heat into the atmosphere, leading to a slight increase in global mean temperature during El Niños. This is only one part of the ENSO contribution to global average temperature, there are other ways of influence that are of more complex nature (Trenberth, Caron, et al., 2002). It has been shown that ENSO accounts for short-term variations in global mean surface temperature with a range up to 0.39°C. The global average temperature usually lags ENSO with a few months. Trenberth,

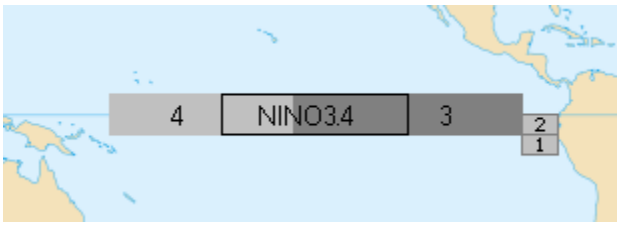

Figure 2.1: The geographical region where the NINO3.4 index is recorded.

Caron, et al. (2002) report that warming events usually lag the NINO3.4 index with three months. Johansson et al. (2015) find that two months maximizes correlation between the NINO3.4 index and SSTs, whereas for land temperatures six months gives the highest correlation.

2.2 The Atlantic Multidecadal Oscillation index

The Atlantic Multidecadal Oscillation (AMO) is a mode of variability with a much longer periodicity than ENSO; around 60 years. It has been credited for droughts and variations in river streamflows in North America, as well as increases in intensity and/or frequency of Atlantic hurricanes (Rogers and Coleman, 2003; Trenberth and Shea, 2006). The reasons behind the AMO are not well known, but its main expression is in SSTs in the North Atlantic Ocean. Both observations and modeling have indicated that the warming of the surface water during the warm phase is accompanied by cooling of the deeper ocean in the tropical North Atlantic (C. Wang and Zhang, 2013). As mentioned in section 2.5 there are several studies suggesting external forcing as a potential driver of the AMO. Another popular theory is that the AMO is induced by variations in the Atlantic meridional overturning circulation[1] (AMOC) (C. Wang and Zhang, 2013).

Traditionally the index has been calculated as mean SSTs in the North Atlantic, north of the equator, and south of 60°N, to avoid problems with sea ice changes. It has often been linearly detrended to highlight the variability. However, the definition used here is from Trenberth and Shea (2006). They argue that simply detrending the data will not remove undesirable influences on the index such as global warming and volcanic eruptions. Instead they subtract the global (60°S-60°N) mean SST from the North Atlantic (0-60°N, 0-80°W)[2] SST, and obtain a revised AMO index which more clearly shows the regional variability. This definition has since been the more commonly used one.

2.3 The Pacific Decadal Oscillation index

The Pacific Decadal Oscillation (PDO) is essentially a long-term El Niño-like pattern, with warm temperatures in the eastern and cool temperatures in the western Pacific. Except from the periodicity, the PDO also diverts from ENSO in that it is mostly seen in the Northern Pacific, with secondary effects in the tropical Pacific, while for ENSO the opposite is true (Mantua, 2003). Most importantly it has a much longer periodicity than ENSO, around 40-60 years. Due to problems with

[1] The main part of the AMOC is the Gulf Stream, and the associated North Atlantic deep water formulation.

[2] This includes the entire North Atlantic Ocean, from the Gulf of Guinea in the southeast, the Caribbeans in the southwest, the Shetland Islands in the northeast, and the North American coastline in the northwest.

multicollinearity[3] with ENSO, the PDO is not used in this study. It has however been used extensively in earlier papers, as mentioned in section 2.5 of this thesis.

2.4 The equilibrium climate sensitivity

The ECS is a parameter indicating the change in GMST implied by a doubling of the pre-industrial atmospheric CO_2 concentration[4]. The unit used here of the ECS is degrees Celsius[5]. A similar parameter is λ, which indicates the change in GMST implied by a unit change in radiative forcing (RF). The unit of λ is C W^{-1} m^2. Since a doubling of the CO_2 concentration is approximately equivalent to an increase of RF by 3.71 W m^{-2}, the relationship between the two parameters is ECS $= 3.71 \cdot \lambda$. The relationship between λ and radiative forcing can be expressed as

$$T_{\text{eq}} = \lambda \cdot \mathcal{F} \tag{2.1}$$

where T_{eq} is the equilibrium change in GMST and $\mathcal{F}$ is radiative forcing. This is further discussed in section 3.1.

As mentioned in chapter 1 it is hard to quantify the ECS due to a number of reasons. However, as Rahmstorf (2008) states, had it not been for feedbacks in the climate system, the ECS would be easily calculated to be equal to 1°C. These feedbacks include:

- The water vapor feedback: Water vapor in the atmosphere accounts for a large percentage of the greenhouse effect, and as temperature rises more water vapor will be present. Therefore this is a positive feedback.
- The ice-albedo feedback: Ice and snow on Earth's surface increases its albedo (reflection coefficient), and reduces the amount of solar energy absorbed. A warmer climate decreases the area of Earth covered by ice and snow, which reduces the albedo and creates a positive feedback.
- The cloud feedback: Clouds affect the radiative forcing in different ways. They reflect incoming shortwave radiation out into space, but on the other hand they also send longwave radiation from below back to the surface. Presently the net effect is a negative feedback but when temperature increases this might change (C. Zhou et al., 2013).
- The lapse rate feedback: Atmospheric temperature decreases with altitude, and the rate of this decrease is known as the lapse rate. It is widely believed that the lapse rate will change and the atmosphere will take up heat more rapidly than the surface. This would contribute to less surface warming, thus creating a negative feedback (Boucher et al., 2013).

[3]When a number of explanatory variables are highly correlated, their coefficients might change erratically, which can lead to invalid results regarding the importance of said variables.

[4]The pre-industrial atmospheric CO_2 concentration was approx. 280 parts per million by volume (ppmv) (Rahmstorf, 2008). In April 2015 the concentration had reached 401.24 ppmv (Dlugokencky and Tans, 2015).

[5]This is equivalent to using degrees Kelvin.

A simple estimate of the ECS from observations is compiled by Rahmstorf (2008). The GMST has increased by roughly 0.8°C and the RF due to anthropogenic GHGs has increased by roughly 2.6 W m^{-2} since 1750 (i.e., before the industrial revolution sparked the observed increase of atmospheric CO_2). Combining this with observations of increased ocean heat content, as well as aerosol and solar radiation changes, one can get a crude estimate of the ECS. The glaring fact that the climate system has not reached its equilibrium does however put a major dent in the reliability of this estimate.

Another way to estimate the ECS is through the use of very sophisticated and computationally intensive models simulating Earth's climate system. The growing power of computing technology makes more advanced models possible. Many possible combinations of parameters, indicating different responses from clouds and other mechanisms, are tested and evaluated based on how well they compare to observations. Literature on this subject is extensive, and some of it is recapped in the following section.

2.5 Literature review

The apparent hiatus in global warming has been studied frequently in recent years. Kosaka and Xie (2013) identify two schools of primary thoughts. One focusing on changes in external forcing, and one focusing on internal climate variability (ICV). Furthermore, Cowtan and Way (2014) explain the hiatus in the HadCRUT4 dataset (see section 4.1 Data) with data coverage gaps, as they suggest that some oversampled regions could have different temperature trends than undersampled ones, such as the polar regions. However, Gleisner et al. (2015) argue that this fact "cannot explain the observed differences between the hiatus and the prehiatus period". Instead they find that the temperature trend 2002-2013 is lower than 1985-1997 especially near the equator.

Research focusing on long-term internal variability as the main reason for the hiatus has been dominant lately. Kosaka and Xie (2013) report that low frequency Pacific variability has reduced global warming in the 21st century, and it similarly accelerated the observed warming from the 1970s to the late 1990s. They do not use any established NINO indices, instead they use sea surface temperatures from a large region (8.2% of the earth's surface) in the central-eastern equatorial Pacific, and find a significant "La Niña-like decadal cooling" in that region during the 21st century. England et al. (2014) find the answer to be blowing in the wind, as they argue that a strengthening in Pacific trade winds over the past two decades can fully explain the surface warming hiatus. As explained in section 2.1, the Pacific trade winds are closely tied to the ENSO cycle, and therefore this result is quite similar to that of Kosaka and Xie (2013). Trenberth and Fasullo (2013) conclude that the positive phase of the PDO during the late 20th century enhanced the surface warming, and similarly its negative phase is cooling the surface somewhat, but it also contributes to an overall warming of the oceans. Yao et al. (2015) also find that the PDO is significant, but that it is leading the multidecadal variability of the surface mean

temperature by approximately 16 years. The AMO on the other hand is found to be largely in phase with the multidecadal variability of the temperature. This result, that the PDO and the AMO are of similar periodicity but not in phase with each other, is in accordance with the "stadium wave" hypothesis presented by Wyatt et al. (2012). Since the AMO is only in the beginning of its decreasing phase, this result suggests that "it is very likely that the current observed slowdown in the rate of global warming will extend for several more years" (Yao et al., 2015). This is in contrast to C. D. Roberts et al. (2015) who use global climate models from the fifth phase of the Coupled Model Intercomparison Project (CMIP5) and a probabilistic approach to determine the likelihood of the current hiatus continuing another five years to be up to 25%. Watanabe et al. (2014) split the surface temperature change into one part caused by internal climate variability, and one anthropogenic part. In the internal climate variability they find a cooling trend around the equator, especially in the eastern Pacific. The previously mentioned findings of Gleisner et al. (2015) are in line with this, as they also find a cooling trend close to the equator. The hypothesis that internal variability is behind the pause in surface warming is backed up by research showing that the deep ocean continues to heat up, throughout the start of the 21st century (Chen and Tung, 2014; Roemmich et al., 2015). Examining subsurface temperature and salinity data, Chen and Tung (2014) find that a recurrent salinity anomaly in the North Atlantic, closely tied to the AMO, has recently led to an increase in heat uptake by deep ocean layers. They predict that these planetary heat sinks will remain intact and the hiatus continue on a decadal time scale.

Some papers use a combination of changes in external forcing and ICV to explain the hiatus. Foster and Rahmstorf (2011) removes the noise caused by the ENSO cycle, volcanic aerosols and the solar cycle, to find that the warming trend continues throughout 2000-2010. Similarly, Johansson et al. (2015) attribute the hiatus to ENSO-related variability and reduced solar forcing. However, this is not the main focus of their study; they focus on how estimates of the ECS change as observations over the hiatus are included. It is found that the most likely value of the ECS has decreased, but this can be due to sources of internal variability not included in their framework. The estimates of the ECS have also fluctuated in the past as observations have accumulated. Douville et al. (2015) show that many climate models overestimate the influence of ENSO, which negatively affects their ability to reliably capture the influence of the tropical Pacific ocean's contribution to the hiatus. Furthermore they point out that model results can be quite sensitive to experimental designs. Their model, which overrides wind stress to control the tropical Pacific ocean heat uptake, partly captures the recent slowdown of global warming, but overestimates global warming overall.

Research focusing on changes in radiative forcing includes Kaufmann et al. (2011), who attribute both the current hiatus and the 1940-1970 cooling period to a large extent to the fact that sulfur emissions increased more than, or as much as, greenhouse gas emissions during these periods. Since 1970 extensive efforts have been made to reduce air pollution, which they claim reduced the aerosol cooling effect

and led to the heavy global warming that evidently was present during 1970-2000. Finally, a recent increase in coal burning in Asia, and China in particular, has again led to sulfur and greenhouse gas emissions canceling each other out as drivers of the global mean temperature. Booth et al. (2012) are of a similar opinion as they argue that "aerosol emissions and periods of volcanic activity explain 76 per cent of the simulated multidecadal variance in detrended 1860–2005 North Atlantic sea surface temperatures". They suggest that it is in fact anthropogenic aerosol radiative forcing that is the origin of the AMO-like temperature cycle seen over the 20th century. Wilcox et al. (2013) extend their result to the global scale. However, using records of tree rings and ice cores, several papers (Delworth and Mann, 2000; Gray et al., 2004; Chylek, Folland, et al., 2012) have found evidence for AMO-like cycles going back several centuries; long before anthropogenic effects on climate were of any significance. Similarly, as a response to Booth et al. (2012), Tung and J. Zhou (2013) use the Central England Temperature (CET), a temperature series going all the way back to 1659, to show that multidecadal variability is present before the industrial revolution as well and hence can not be explained by anthropogenic aerosol emissions. Instead they claim that this recurrent multidecadal oscillation is likely an internal variability related to the AMO. Still, there is research claiming that even before any anthropogenic influence on the climate, external forcing from volcanic aerosols and the variability of the solar cycle, could have played a role in pacing internal variability (Otterå et al., 2010; T. Wang et al., 2012; Knudsen et al., 2014). In J. Zhou and Tung (2013) they continue to show that when including the AMO in a multiple regression analysis, similar to that of Foster and Rahmstorf (2011), there is no evidence of a hiatus in the anthropogenic warming, but the warming trend is reduced by a factor of at least two. Related to this are the findings of Chylek, Klett, et al. (2014), who state that most climate models are unable to simulate the AMO cycle. Still some CMIP5 models reproduce the AMO-like cycle with correct timing. However, they show that this behavior is due to an overestimation of aerosol effects, which leads to the anthropogenic component cooling the system between 1950-1970. IPCC's AR5 concludes that it remains uncertain how much of the decadal temperature variations that is attributed to the AMO in some studies that is actually related to external forcing (Bindoff et al., 2013). The same report states that more certain is the fact that the contribution of the AMO to global warming since 1951 is considerably less than 0.1°C, and that it is "virtually certain that internal climate variability alone can not account for the observed global warming" since the middle of the 20th century.

Some, but not all, of the papers mentioned here provides estimates of the ECS. There are also numerous papers estimating the ECS without any specific focus on the recent hiatus. As mentioned in chapter 1, IPCC's AR5 summarizes estimates up to 2013, stating that the ECS is "likely between 1.5°C and 4.5°C" (Bindoff et al., 2013). One of the lower recent estimates is given by Skeie et al. (2014) who report an estimate for the corresponding interval of (0.92, 3.18). At the other end of the spectrum is Sherwood et al. (2014) who report a lower bound of 3°C, with a most likely value of 4°C. The sensitivity of the estimate to which temperature dataset is used is highlighted by Libardoni and Forest (2011).

Concerning the methods used for climate research, most research in the past decades[6] has been centered on the use of coupled atmosphere-ocean general circulation models (AOGCMs). These models are usually large and complex, whose primary function is to understand the dynamics of the physical constituents of the climate system (atmosphere, ocean, land and sea ice), and for making projections based on future greenhouse gas and aerosol forcing (Flato et al., 2013). Lately, third-generation GCMs known as earth system models (ESMs) have been developed, which incorporate interactive biochemistry, including the carbon cycle (Dunne, 2014). As stated earlier, virtually no climate models were able to predict the hiatus (Fyfe et al., 2013; C. D. Roberts et al., 2015). This is a contributing reason to that recently empirical statistical models have been used more frequently, to complement physics-based models (Chylek, Klett, et al., 2014). Some papers use statistical methods exclusively (e.g. Foster and Rahmstorf, 2011; Wu et al., 2011; Chylek, Klett, et al., 2014; Yao et al., 2015), some pair it with GCMs (C. D. Roberts et al., 2015), and some use statistics in combination with simpler physics-based models (Tomassini et al., 2007; Aldrin et al., 2012; Skeie et al., 2014; Johansson et al., 2015).

This thesis will look to join the latter group, as a simple energy balance model is combined with regression and Monte Carlo methods, to continue investigating the explanations behind the interdecadal temperature oscillations we have seen during the past century. The aerosol forcing path will be allowed to vary and different internal climate variability indices will be included, and the effects on the climate sensitivity parameter will be examined. Many authors who perform similar analyses account for interannual variability by including ENSO in their analysis. Including interdecadal variability is not as frequently seen; it is done by Skeie et al. (2014), but they base their long-term variability on a combination of GCM simulations and data. Here the long-term variability will be based solely on data from the AMO index. The flexibility in the aerosol path considered here has to the knowledge of this author not been included in any earlier studies of similar nature.

[6] General circulation models (GCMs) were initially developed in the 1950s and 1960s, and the first AOGCM was developed by Manabe and Bryan in 1969 (Edwards, 2001).

3
Theory

This chapter explains the key theoretical concepts on which this study is built. Some examples of previous literature in this field using the same concepts are also given.

3.1 Energy balance model

An energy balance model (EBM) is a simple climate system model, built on the fact that all incoming energy is either emitted back out into space or absorbed. Following Kriegler (2005) we set F_S to be the infrared radiation from Earth's surface, and note that since Earth's surface radiates like a blackbody, by Stefan-Boltzmann's law we have that $F_S = \sigma T_S^4$ where $\sigma = 5.67 \cdot 10^{-8}$ W m^{-2} K^{-4} is the Stefan-Boltzmann constant and T_S is the surface temperature of Earth. Letting F_{Sol} denote the portion of solar radiation absorbed by Earth and G be the additional energy distributed to Earth's surface due to the absorption of infrared radiation in the atmosphere, we can express energy balance as

$$\sigma T_S^4 = F_{\text{Sol}} + G \tag{3.1}$$

Deviation from this energy balance induces a heat flux at Earth's surface. The net radiative imbalance implied by an external forcing $\mathcal{F}$ and a change in temperature can be expressed as $N = \mathcal{F} - \frac{T}{\lambda}$ (Geoffroy et al., 2013). Here $\mathcal{F}$ includes radiative forcing due to emissions of GHGs, changes in solar radiation, and atmospheric aerosols. The other term, $\frac{T}{\lambda}$ includes the temperature feedback. When this system reaches its steady-state, $N = 0$, we get $T_{\text{eq}} = \mathcal{F}\lambda$. This is equivalent to the definition of the climate sensitivity parameter λ in section 2.4; λ is the equilibrium temperature implied by a unit change in RF.

A logical next step to extend this very simple EBM is to describe how the heat accumulated by Earth is distributed. This is commonly done by adding the deep ocean to the model. An example is the two-box EBM used by Geoffroy et al. (2013) where the heat exchange between the surface- and deep ocean box is assumed to be proportional to the difference between the temperature perturbations of the two boxes. The model employed for this study is similar but slightly more advanced; the deep ocean box is split into several layers, whose heat exchange is modeled by one-dimensional diffusion, with uniform diffusivity. The ocean surface water, land, and the atmosphere is combined into the well-mixed surface box. Similar models have been studied in Wigley and Schlesinger (1985), Kriegler (2005) and Johansson

(2011). The model is described by the following set of equations:

$$C_s \frac{\partial T(0,t)}{\partial t} = \mathcal{F}(t) - \frac{T(0,t)}{\lambda} - F_d \qquad ,\forall t \geq 0 \tag{3.2}$$

$$\frac{\partial T(z,t)}{\partial t} = \kappa \frac{\partial^2 T(z,t)}{\partial z^2} \qquad ,\forall t \geq 0, z > 0 \tag{3.3}$$

$$F_d = -\rho c \kappa \left(\frac{\partial T(z,t)}{\partial z} \right)_{z=0} \qquad ,\forall t \geq 0 \tag{3.4}$$

Equation (3.2) describes the surface box, equation (3.3) describes the diffusion between layers in the deep ocean box, and equation (3.4) describes the heat flux between the surface box and the upmost layer of the deep ocean box. The temperature at time t and layer z of the deep ocean box is denoted $T(z,t)$, and $T(0,t)$ is the temperature of the surface box. The radiative forcing at time t is $\mathcal{F}(t)$. We have the initial condition $T(z,0) = 0$, $\forall z \geq 0$, and the boundary condition

$$\left(\frac{\partial T(z,t)}{\partial t} \right)_{z=z_B} = 0, \forall t \geq 0 \tag{3.5}$$

at the bottom of the ocean. We have that $C_s = c\rho h$ where h is the effective depth of the surface box, c is the specific heat capacity of water (4186 J kg^{-1} K^{-1}), and ρ is the density of salt water (1027 kg m^{-3}). Finally κ is the effective diffusivity of heat in the deep ocean. The role of each parameter is further discussed in section 4.5.

3.2 Bayes' theorem

Bayes' theorem for distributions takes the following form:

$$p(\theta|y) \propto \mathcal{L}(y|\theta) \cdot p(\theta) \tag{3.6}$$

Here θ is a set of parameters, and y is data. $p(\theta)$ is the a priori probability density function (PDF), and $p(\theta|y)$ is the a posteriori PDF, where the likelihood $\mathcal{L}(y|\theta)$ of the data y given the parameters θ, has been taken into account. This is useful when one has a vague sense of the distribution of a parameter, and data is available. The theorem gives a way to combine prior knowledge and new evidence into a better estimate, the posterior distribution.

3.3 Markov chain Monte Carlo methods

Posterior distributions of parameters are often hard to sample from directly. Markov chain Monte Carlo (MCMC) methods are algorithms that make this possible by constructing a Markov chain which converges to the desired distribution. MCMC methods have been used before in this type of research, for example in Titus and Narayanan (1996), Tomassini et al. (2007), Aldrin et al. (2012), Skeie et al. (2014) and Johansson et al. (2015). The algorithm used in this study is the Metropolis

algorithm, proposed by Metropolis et al. (1953). In line with previous research, it is assumed that the parameters are independent of each other in the a priori distribution. This greatly simplifies the generation of samples in the Metropolis algorithm, which can be done by random-walk updating. A description of the algorithm follows:

1. Let θ_i be the current set of parameters, and θ_{new} the proposal for new parameters. The new parameters are drawn from a proposal distribution $Q(\theta_{\text{new}}|\theta_i)$ which is in this study chosen to be $\mathcal{N}(\theta_i, \nu)$. Here ν is the covariance matrix, but since all parameters are assumed independent of each other, it is filled with zeros everywhere except for on its diagonal. The diagonal is a vector of variances. The magnitudes of these variances are discussed below.

2. The probability of accepting this new set of parameters is calculated by

$$p = \frac{f(\theta_{\text{new}})}{f(\theta_i)} \tag{3.7}$$

   where f is a PDF proportional to the PDF of the desired, posterior, distribution. If $p \geq 1$ then the new parameters are accepted, and $\theta_{i+1} = \theta_{\text{new}}$. If $p < 1$ then the new parameters are accepted with the probability p. If the candidate is rejected, then $\theta_{i+1} = \theta_i$.

To get a sample which well resembles the distribution, one usually discards the first iterations, known as the *burn-in* period. The parameter values during this period might be too influenced by the starting values, θ_0. The length of the burn-in period is influenced by the step size, i.e., the magnitude of elements in ν. With small steps, the burn-in period should be quite long. Also, a set of nearby steps will always be correlated with each other. Therefore one could throw away some observations and only look at every kth sample, known as "thinning". It has been noted that thinning rarely is an efficient way of getting better samples (MacEachern and Berliner, 1994; Link and Eaton, 2012). It does not significantly effect the posterior distribution, but it can be beneficial as smaller datasets are easier to work with.

Choosing the sizes of variances in the proposal distribution is a very important step in designing the Metropolis algorithm. If the variances are too large, the algorithm will attempt to take large steps. This will have the consequence that the random walk will quite quickly come close to its optimal state. This might sound beneficial, but once it is there, very few proposed parameters will be accepted, since they will be very far away from the optimal state, and therefore give a much smaller likelihood. Hence the random walk will not give a good representation of the full posterior distribution. The acceptance rate is the fraction of the proposed parameters that are accepted, and it would in the case of very large variances be too low. On the other hand, too small variances implies a slow random walk, which will take a very long time to explore the full distribution. G. O. Roberts et al. (1997) show that if both the target posterior distribution and the proposal distribution $Q(\theta_{\text{new}}|\theta_i)$ are normal, then the optimal acceptance rate is roughly 25% for dimensions higher than two. There is no established way of estimating the acceptance rate for a given covariance matrix ν beforehand, so it is commonly updated by trial-and-error until a satisfactory acceptance rate has been obtained.

3.4 Regression

Linear regression is used to model the relationship between a dependent variable and one or more explanatory variables. The dependent variable is approximated by a linear combination of the explanatory variables:

$$y_i = \sum_{j=1}^{m} \beta_j x_{i,j} + \epsilon_i, i = 1, ...n \tag{3.8}$$

where n is the number of observations and m the number of explanatory variables. β_j is the regression coefficient for the jth variable, $x_{i,j}$ is the ith observation of the jth variable, y_i is the ith observation of the dependent variable, and ϵ_i is the error term for the ith observation.

It is often of great interest to check whether an explanatory variable really helps explaining the dependent variable. Here the null hypothesis $H_0 : \beta_j = 0$ will be used. If this hypothesis can be rejected with a good amount of confidence, then we can say that there is significant linear correlation between the jth explanatory variable and the dependent variable. The significance level is denoted α and it is defined as the risk of rejecting H_0 when it is in fact true. If the $(1 - \alpha) \cdot 100\%$ confidence interval for β_j does not contain 0, then β_j is significant at the α significance level. Common values for α are 0.10, 0.05 and 0.01.

4
Methods

This chapter first describes the data used in this study, and then explains and motivates the methods that are employed.

4.1 Data

Radiative forcing due to greenhouse gases is taken from Meinshausen et al. (2011)[1]. This data only covers the period 1765-2005, but it is extended to 2006-2013 with the RCP4.5 scenario[2], which is close to the actual development. Similarly to Johansson et al. (2015), the total anthropogenic aerosol forcing (including direct aerosol forcing, aerosol cloud interaction and black carbon on snow) is treated together. Data for this too is taken from Meinshausen et al. (2011). Volcanic forcing is for the period 1765-1849 also taken from Meinshausen et al. (2011). For 1850 and onwards it is taken from Goddard Institute for Space Studies (2015). Unfortunately, this dataset ends in September 2012, so for the final 15 months the volcanic forcing is set to zero. Solar radiative forcing is taken from Meinshausen et al. (2011) for 1765-1978. For 1979-2013 total solar irradiance data is taken from Fröhlich (2000)[3], and converted to radiative forcing using an approximate earth albedo of 0.3. The radiative forcing data can be seen in Figure 4.1. A closer look on said figure reveals that the solar cycle was in its negative phase approximately 2005-2013, which as stated in section 2.5 has been mentioned as part of the explanation of the current hiatus. This negative phase was actually an unusually significant one, with 2010 being the lowest yearly average of measured solar irradiation since 1933.

Ocean heat content (OHC) is defined as the heat stored in the oceans, and it is given in 10^{22} Joules, both in the data and for the rest of this thesis. Data is taken from National Oceanographic Data Center (2015). In this source the OHC is calculated using the upper 2000 meters of the ocean. Measurements began in 1955, and the data is pentadal (5 year) averages. Therefore it is only available for 1957-2012, and hence OHC will only be evaluated on this period. The pentadal observations can be seen as low-pass filtered annual observations, and they are treated as annual observations. For a sensitivity analysis regarding this assumption, see Johansson

[1] Available online, see Meinshausen (2011).

[2] The RCP4.5 scenario is the *Representative Concentration Pathway* that gives a +4.5 W m^{-2} RF value, compared to pre-industrial values, in 2100. Representative Concentration Pathways are projections describing possible climate futures, adopted by the IPCC in 2013.

[3] Available online at `http://climexp.knmi.nl/data/itsi.dat`. Visited on January 22, 2015.

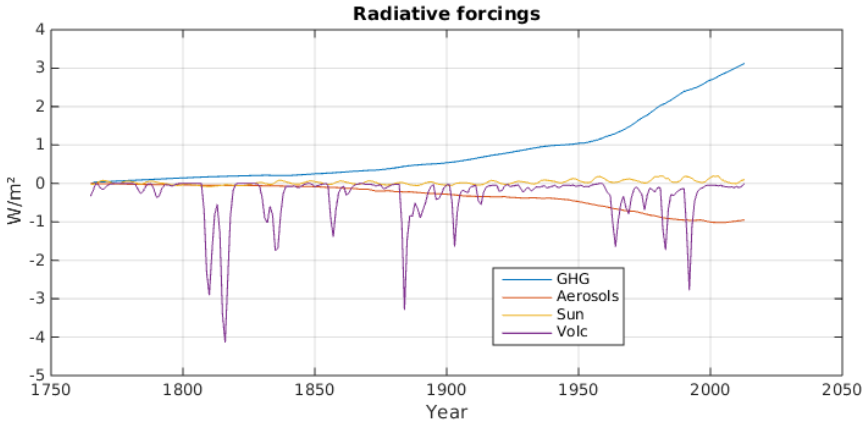

Figure 4.1: Changes in radiative forcing from pre-industrial levels. "GHG" is an abbreviation for greenhouse gases, and "Volc" is volcanic aerosols.

et al. (2015). The OHC data is visualized in Figure 4.2.

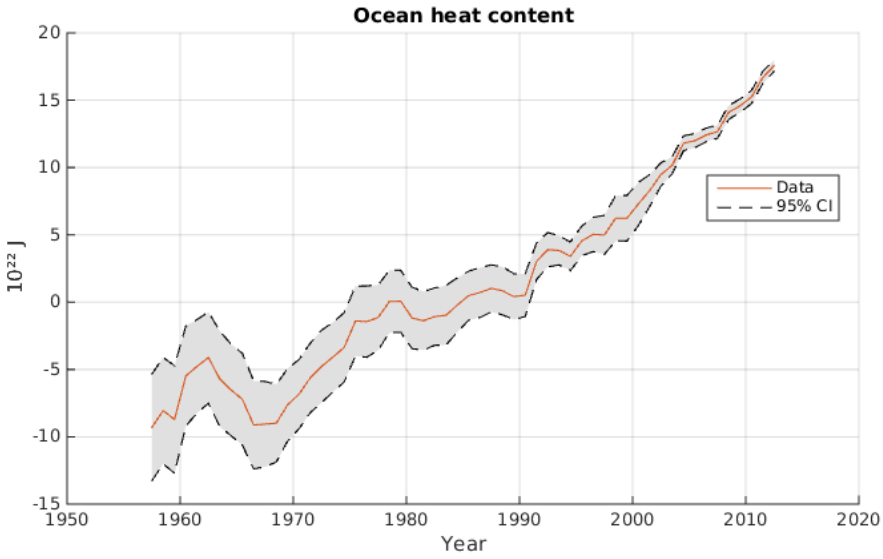

Figure 4.2: OHC data. The confidence intervals are approximate normal, constructed by multiplying the standard errors by 1.96 which gives a confidence level of 95%.

Temperature data is taken from two different sources. The HadCRUT4 data (temperature and temperature uncertainties) is taken from Met Office Hadley Centre (2015). It combines the HadSST3 dataset for sea temperature, and CRUTEM4 for land temperature. The datasets are produced by Met Office Hadley Centre (HadSST) and the Climatic Research Unit of University of East Anglia (CRUTEM), both based in the United Kingdom. The other dataset is produced by the National Oceanic and Atmospheric Administration's (NOAA's) National Centers for Envi-

ronmental Information (NCEI)[4]. This dataset is henceforth referred to as NOAA temperature data, and it is taken from National Climatic Data Center (2015b). It combines SSTs from the ERSST v3b dataset with land temperature from the Global Historical Climatology Network-Monthly (GHCN-M) dataset. The temperature datasets differ in a number of ways; urbanization bias adjustment, measurement bias adjustment, gridding methodology, etc. (Morice et al., 2012). The uncertainty in temperature resulting from the choice of methodology is referred to as "structural uncertainty". Using multiple temperature datasets in studies such as the analysis conducted in this thesis yields the advantage of being able to assess the sensitivity of results to structural uncertainty. Therefore all model evaluations here will be run on both datasets separately. Observational uncertainties are available for both datasets, and they are visualized in Figure B.1 in appendix B.

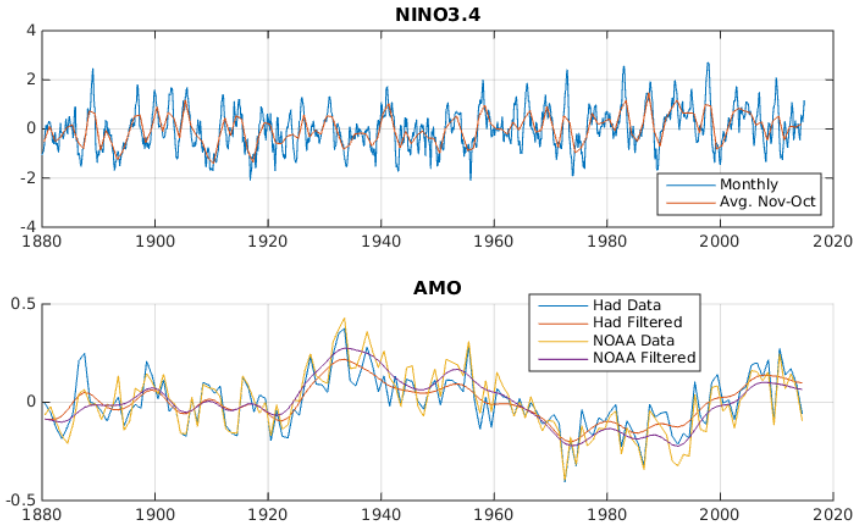

Figure 4.3: Summary of internal climate variability indices.

Internal climate variability indices are also taken from several different sources. To capture ENSO effects the NINO3.4 index will be used. It is calculated from NOAA's ERSST v3b, taken from van Oldenborgh (2015). Again, for a description of the NINO3.4 region see Figure 2.1. Data is monthly, and it is calculated as anomalies in SST over the region from that month's historical mean. In this study, the time scale considered is years, so the data will be annual averages. As discussed in section 2.1, the global temperature lags the NINO3.4 index with a few months. Upon analyzing the correlation (see appendix A.1), it is found that for both temperature datasets two months maximizes correlation with the NINO3.4 index. Hence a two month lag is used when calculating yearly averages, so that the value for year Y is the average from November year $Y-1$ to October year Y. The AMO data is calculated in two ways. We have one time series based on the temperature set

[4]This data was produced by NOAA's National Climatic Data Center (NCDC) until recently, when NCDC merged with the National Geophysical Data Center and the National Oceanographic Data Center into NCEI.

ERSST v3b, the same SST data as the NOAA temperature series is based upon. Even though the global mean has been subtracted from the AMO signal, and the signal has been filtered, there might be correlation based on observational and structural uncertainties between the AMO signal and the temperature data. Therefore calculations will also be carried out with the AMO signal calculated on the SST part of the HadCRUT temperature data (HadSST 3.1.1.0). Both versions are taken from van Oldenborgh (2015). Note that the NINO3.4 data suffers from the same problem, at least at a first glance. It is calculated from the NOAA temperature dataset, and there is a risk that there is correlation between the NOAA temperature and this NINO3.4 data that stems from observational or structural uncertainty. However, upon examining the correlations (again, see appendix A.1) between the different temperature datasets and the ERSST NINO3.4 data, it is found that they are very similar. In fact the correlation is slightly larger for the HadCRUT GMSTs, and not the other way around. Therefore it is deemed unnecessary to also analyze NINO3.4 data based on the HadSST temperature data. The time series for both El Niño and AMO are visualized in Figure 4.3.

4.1.1 Filtering

To extract the multidecadal oscillatory part of the AMO signal, it is common to apply a low-pass filter to it. For this thesis, the AMO data is filtered using a 13-term weighted moving average filter, which is used in the IPCC's AR4 (Trenberth, Jones, et al., 2007) and several other papers (Trenberth and Shea, 2006; Trenberth and Fasullo, 2013; Yao et al., 2015). Other filters that have been used for this purpose includes a plain uniform running average filter, for example with length 11 years (Knudsen et al., 2014), or a Butterworth filter (Otterå et al., 2010). Data is annual, so the filtered data point at year i is influenced by the years $i \pm 6$. The weights approximate a normal distribution[5], as seen from the bell-shaped plot of the weights in Figure 4.4. Specifically, the weights are $\frac{1}{576}(1, 6, 19, 42, 71, 96, 106, 96, 71, 42, 19, 6, 1)$. Just as in Trenberth, Jones, et al. (2007), the "minimum slope" constraint of Mann (2004) is used at the beginning and end of each filtering. To approximate this constraint, one pads the time series with values within half the window width of the boundary, reflected in the boundary. In other words, the beginning of the time series $x_t, t \in [0, n]$ will in the case of a 13 term window be padded by $x_6, x_5, x_4, x_3, x_2, x_1$ before the start $(x_0, x_1, ...)$. This reduces the slope of the smoothed series as it approaches the boundary.

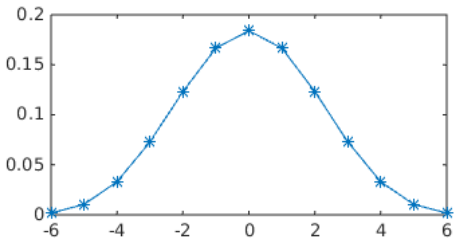

Figure 4.4: Weights for the used filter.

[5] Approximately $\mathcal{N}(0, 2.2^2)$.

4.2 Discretization of the energy balance model

The system described by equations (3.2)-(3.4) is discretized using Euler forward in time. For all $t \geq 0$ we have

$$T(0, t + \Delta t) = T(0, t) + \frac{\Delta t}{C_s}\left(\mathcal{F}(t) - \frac{T(0,t)}{\lambda} - F_d\right) \tag{4.1}$$

$$T(z, t + \Delta t) = T(z, t) + \frac{\kappa \Delta t}{(\Delta z)^2}\left(T(z + \Delta z, t) - 2T(z, t) + T(z - \Delta z, t)\right) \tag{4.2}$$

$$F_d = -\frac{\rho c \kappa}{\Delta z}\left(T(\Delta z, t) - T(0, t)\right) \tag{4.3}$$

where equation (4.2) holds for all $z > \Delta z$. The depth of the deep ocean box is set to $z_B = 4000$ m, and $\Delta z = 100$ m, which has been common in earlier research using similar models (Kriegler, 2005). Even though the data is annual, $\Delta t = 1$ year is too large a timestep, since it leads to instability of the system for this choice of Δz. Therefore $\Delta t = 0.1$ years is used in the numerical integration.

4.3 Evaluating model

After temperature estimates have been obtained using the box diffusion model, estimates of the OHC are calculated. Since the OHC data is calculated from the upper 2000 meters of the ocean, only these layers are used to estimate the OHC, even though there might be more layers present. The heat content of layer z is

$$H = \rho c A h_z T(z, t) \tag{4.4}$$

where A is the area of Earth's oceans[6], and h_z is the height of layer z. The OHC pentadal observations are normalized over the period 1957-1986 (Johansson et al., 2015), but the temperature estimates obtained from the diffusion box model are anomalies from the temperature in 1765. Therefore the estimates and the observations will be offset with some constant. To deal with this the residuals are subtracted by their mean, to make them centered around zero. Finally an autoregressive (AR) term, with lag 1, is also added to the residuals, since autocorrelation is present. AR(1) processes have been used extensively in climate research for modeling internal climate variability (Johansson et al., 2015). The likelihood function is

$$\mathcal{L}_H = \phi(H_{\text{res}}; 0, \sigma_1 + \sigma_h) \tag{4.5}$$

where $\phi(x, \mu, s)$ is the normal distribution PDF evaluated at x, with mean μ and standard deviation s. The observational uncertainty is given by σ_h, which is an exogenous input, and σ_1 is a parameter of the model.

Now, internal climate variability (ICV) is involved. The preferred ICV indices are added linearly:

$$T_{\text{res}}(t) = T_{\text{obs}}(t) - T(0, t) - \sum_{i=1}^{n} \beta_i \cdot \text{ICV}(i) \tag{4.6}$$

[6]The area of Earth's oceans is here approximated to be $360 \cdot 10^6$ km^2.

Here $T(0,t)$ is the calculated temperature at time t of the surface box, and n is the desired number of ICV indices, in our case equal to one or two. Since temperature data is given as anomalies from the mean over some period, which can be different for each data source, the residuals are centered around zero by adding a constant just as for the OHC residuals. Furthermore, the temperature residuals are assumed to follow an AR(1) process, also just as the OHC residuals. The likelihood function looks as follows

$$\mathcal{L}_T = \phi(T_{\text{res}}; 0, \sigma_2 + \sigma_t) \tag{4.7}$$

This is obviously very similar to the OHC case, equation (4.5). The approximate uncertainty of the temperature observations is available for both the HadCRUT and NOAA datasets. To calculate the likelihood of the data given a set of parameters, the two likelihood functions are multiplied:

$$\mathcal{L}(y|\theta) = \mathcal{L}_H \cdot \mathcal{L}_T \tag{4.8}$$

where $\mathcal{L}_H$ and $\mathcal{L}_T$ are calculated with the data y and parameters θ. This value is then inserted into equation (3.6) to obtain posterior parameter estimates.

4.4 Aerosol scaling

There is a great deal of uncertainty surrounding the effects of aerosols on the radiative forcing, as concluded in AR5's eight chapter (Myhre et al., 2013). Especially the cloud albedo effect, and the changes in surface albedo due to black carbon on snow, have question marks surrounding themselves. In this model, as well as many others, a scaling factor w_{aero} is used. This factor is multiplied to all aerosol forcing data, over the entire time domain 1765-2013. However, as Tanaka et al. (2009) states, the historical uncertainty has often been overlooked. In other words, the magnitude of the aerosol forcing is adapted, but the path is still uncertain. To compensate for this, a set of weights are added to this model, to more fully characterize historical forcing uncertainty. A set of breaking points are defined, with 1765 and 1880 being the two first ones. Then between the years 1880-2013, a breaking point is added every 20 years. Finally each observation of aerosol forcing is multiplied by a linear combination of the weights of its two closest breaking points. In other words, the aerosol scaling is not constant, but piecewise linear over time. If we have J break points, then for every break point j between 1 and $J-1$:

$$\hat{a}(i) = a(i)\frac{w_j \cdot (m_j - i) + w_{j+1} \cdot i}{m_j} \qquad , 0 \leq i < m_j \tag{4.9}$$

$\hat{a}(i)$ - Scaled aerosol value at time t.
$a(i)$ - Pre-scaling aerosol value at time t.
m_j - Years between break point j and $j+1$.
w_j - Weight at break point j.

So if for example there are break points at years 1960 and 1980, then the aerosol weight at year 1967 would be $\frac{7}{20}w_{1980} + \frac{13}{20}w_{1960}$. It is important to keep in mind that

the aerosol scaling function over time will still be multiplied by w_{aero}, a constant with a much wider prior than the time dependent weights. The priors of the time dependent weights should be kept narrow as there is only brief insecurity in the aerosol path, but plenty of insecurity regarding its magnitude.

4.5 Parameters and priors

In this section, the parameters and their prior distributions are described. Priors should be informative for the parameters where one has certain knowledge, and vague for others. For some parameters we do not want to constrain the posterior distribution very much, but still there is no need to allow for values that are far from credible. A summary of all parameters can be found in Table 4.1.

Notation	Name	Unit	Prior
σ_1	Std. dev. of temperature	C	U(0,∞)
σ_2	Std. dev. of OHC	10^{22} J	U(0,∞)
λ	Climate sensitivity parameter	C m^2 W^{-1}	U(0,5)
κ	Diffusivity	m^2 s^{-1}	U($10^{-5}, 10^{-3}$)
h	Effective depth of surface box	m	U(10,100)
$\zeta_{h,t}$	AR(1) terms	-	U(-1,1)
β_i	Coefficients for ICV	-	U(-1,1)
w_{volc}	Weight of volcanic RF	-	ln $\mathcal{N}$(-0.187,0.404^2)^a
w_{aero}	Weight of aerosols	-	$\mathcal{N}$(1,0.6^2)
w_y	Weight of aerosols around year y	-	$\mathcal{N}$(1,0.1^2)

Table 4.1: Model parameters, with prior distributions. Note that all uniform priors are on **open** intervals.
a - Corresponds to mean 0.9, standard deviation 0.379.

The prior of the climate sensitivity parameter λ is in earlier work usually uniform over a large interval, and this is the case here as well. The upper limit of 5 C m^2 W^{-1} includes even the highest outlier estimates of this parameter. From section 2.4 we have that ECS = $3.71 \cdot \lambda$, so $\lambda = 5$ C m^2 W^{-1} corresponds to ECS = 18.55°C. The different estimates of the ECS summarized in IPCC's AR5 chapter 10 (Bindoff et al., 2013), all have the 95th percentile lower than 10°C, so the prior used here should be wide enough.

The vertical diffusivity parameter κ decides how quickly heat is taken up by the oceans. The higher the diffusivity, the more rapidly energy is driven down into the oceans. Therefore a high diffusivity also means that the surface temperature will show a slower response to increased external forcing (Johansson, 2011). The parameter has a uniform prior on ($10^{-5}, 10^{-3}$) m^2 s^{-1} or (0.1,10) cm^2 s^{-1}. In Johansson (2011) values between 0.5-3.0 cm^2 s^{-1} are used, and Kriegler (2005) finds that high likelihoods are concentrated at κ below 2 cm^2 s^{-1}. However, the IPCC's working group I third assessment report (TAR) states that it can be as large as 9 cm^2 s^{-1}

(Cubasch et al., 2001), hence the width of this prior.

The depth h of the mixed ocean box plays the following role in the model. Since this box is the upmost one it is the most responsive to changes in external forcing on short time scales. The deeper it is, the more it will contribute to the estimated OHC. In other words, a larger h means that the estimated OHC reacts quicker to changes in external forcing. As Johansson et al. (2015) states, h is usually set to 50-75 meters in globally aggregated EBMs. Since we do not want to constrain it very much the prior is set to U(10,100).

The AR terms ζ_h and ζ_t have uniform priors on (-1,1). The prior can not be wider than this, because an AR(1) process where the absolute value is larger than one is unstable. Hence all information in the posterior distribution of these parameters will come from data.

As stated earlier the total anthropogenic aerosol forcing (including direct aerosol forcing, aerosol cloud interaction and black carbon on snow) is treated together. The estimates in IPCC AR5 chapter 8 indicates plenty of uncertainty regarding this data (Myhre et al., 2013). A 90% interval of -1.9 to -0.1 W m^{-2} is reported, with a best estimate of -0.9 W m^{-2}. This corresponds approximately to a 90% interval for the weight between $\frac{-0.1}{-0.9} = 0.11$ and $\frac{-1.9}{-0.9} = 2.11$. Note that this distribution is not quite symmetric. For simplicity a normal distribution will be used here, centered around 1 since there is no immediate reason to distrust the data. A standard deviation of 0.6 corresponds to the 90% interval (0.013, 1.987) which is deemed close enough to (0.11, 2.11). It has been noted (Johansson, 2011) that statistically this parameter tends to follow λ in energy balance models. This is very intuitive; the higher the climate sensitivity, the more negative the aerosol forcing must be for the estimated temperature to follow the historical temperature. The same paper states that the opposite relationship can be seen between the aerosol weights (w_{aero}, w_{volc}) and the diffusivity κ. As mentioned above, a low heat diffusivity is tied to a faster temperature response. Therefore, to fit modeled GMSTs with data, the net aerosol forcing has to be relatively large for a given λ.

The aerosol path weight priors are centered around one, with a standard deviation of 0.1, which allows for some flexibility in the path. In Figure 4.5 the resulting prior aerosol path uncertainty is visualized. The path can vary inside the intervals, and is then multiplied by w_{aero} to adapt the magnitude.

The volcanic forcing is specifically tied to the diffusivity, depth of the mixed layer, and the ECS, since volcanic aerosols is the source of radiative forcing that is most likely to change dramatically on short notice. A low (high) diffusivity, i.e., quick (slow) temperature response, would mean that volcanic eruptions are more (less) clearly noticeable in the GMST, for given values of h and the ECS. The uncertainty of volcanic aerosol forcing is not clearly reported in IPCC AR5. Hence the estimate of Tomassini et al. (2007) will be used, i.e., a lognormal distribution with mean 0.9 and standard deviation 0.379.

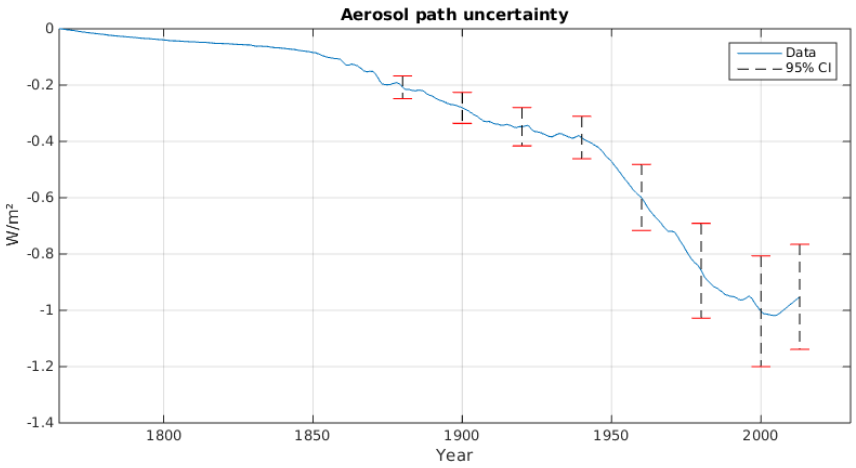

Figure 4.5: The prior aerosol path uncertainty for the assumed standard deviation of 0.1. Plotted are the 95% confidence intervals at each break point.

5
Results

The Metropolis algorithm is run with a few different proposal distributions, where the variances are tweaked until a satisfactory acceptance rate is obtained. The average acceptance rate for the proposal distribution ultimately chosen is around 25-30% for all evaluations. For each model configuration the Metropolis algorithm is run with $n = 5 \cdot 10^6$ iterations, where the $2 \cdot 10^5$ first observations are discarded as the burn-in period, whose length is determined by visual examination of the random walks. To begin with, the model is run for both temperature datasets without any ICV. Then ICV is added, first ENSO for interannual variability, and then the AMO for interdecadal variability. AMO data is first taken from the ERSST dataset, the same as the NOAA temperature data and the ENSO data is calculated from. As mentioned earlier, calculations are also carried out using another AMO data source, the HadSST temperature dataset. The results of these calculations are presented in section 5.1. As a sensitivity analysis on the variable aerosol path, all calculations are also carried out with fixed aerosol path. The results of these calculations are presented in section 5.2. In this chapter models that do not include any internal climate variability are referred to as "No ICV". Models including ENSO but no interdecadal variability are referred to as "ENSO", and models also including AMO are referred to as "ENSO+AMO".

When adding ICV one must pay attention to the regression coefficients to see whether they are statistically significant or not. The ENSO coefficients β_{ENSO} are

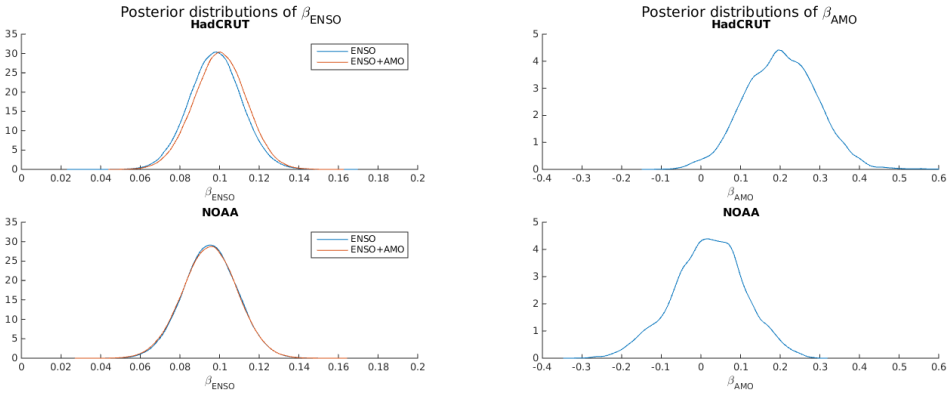

Figure 5.1: Posterior distributions of β_{ENSO} (left) and β_{AMO} (right) for different model configurations.

significant for every model configuration, as seen from the posterior distributions in

Figure 5.1. For all the distributions the probability of $\beta_{\text{ENSO}} = 0$ is infinitesimal, so we can reject the null hypothesis that there is no significant linear correlation between the EBM temperature residuals and the NINO3.4 index. However, this can not be said for the AMO coefficients β_{AMO}. For the HadCRUT temperature dataset β_{AMO} is significant at the $\alpha = 0.05$ level. For the NOAA temperature dataset on the other hand, β_{AMO} is not significant at all, even though the AMO data is taken from a dataset which the NOAA temperature data is partly based upon. Therefore, the results given by the model based on NOAA temperature data and including AMO might not be very interesting, since the crucial assumption that the AMO affects the surface box temperature does not seem to hold.

The posterior densities of the ECS are visualized in Figure 5.2. Overall, a pattern can be seen where the HadCRUT temperature data is associated with higher posterior values of the ECS than the NOAA data. Also, the posterior distributions using the HadCRUT GMSTs are generally wider, with a heavier right tail. In Table

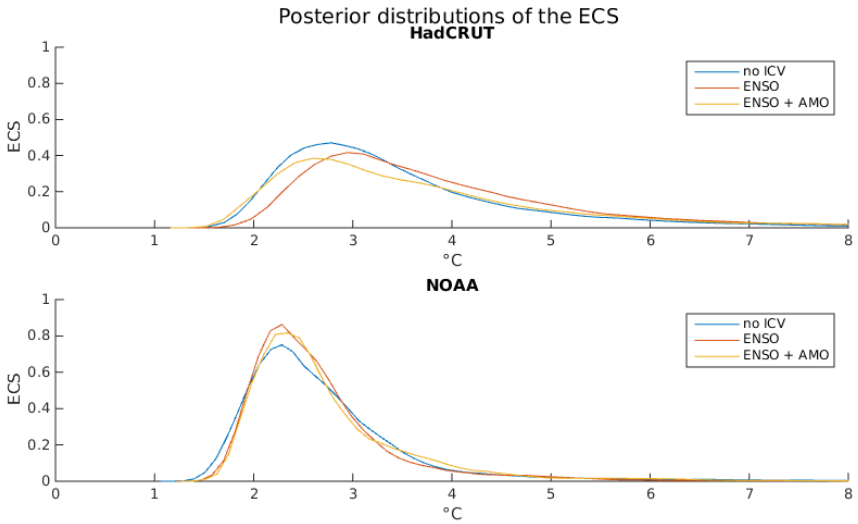

Figure 5.2: Posterior distributions for the equilibrium climate sensitivity, for different model configurations.

5.1, 90% credible intervals of the ECS are shown. This is convenient for comparison with estimates from previous research. The table reveals that the right tail of the ECS posterior for the HadCRUT ENSO+AMO model is especially heavy, which is not easily seen in Figure 5.2. The probability that the ECS is greater than 10°C is 10 times greater when both ENSO and AMO are considered, compared to when none of them are, for both temperature datasets. Again, the difference between temperature datasets is substantial, as for any given model $P(\text{ECS} > 10)$ is more than 10 times greater when the HadCRUT dataset is used compared to when the NOAA dataset is used.

The posteriors of the scale factor for anthropogenic aerosols, w_{aero}, is visualized in Figure 5.3. As expected they follow the posteriors of the ECS, with higher values for HadCRUT than NOAA temperature data. It also seems that including ICV

Temp. dataset	Model	5th perc.	Mode	95th perc.	$P(\text{ECS} > 10)$
HadCRUT	no ICV	2.11	2.73	6.33	0.0058
	ENSO	2.34	3.00	7.56	0.0210
	ENSO+AMO	2.07	2.55	11.58	0.0617
NOAA	no ICV	1.80	2.32	4.43	0.0004
	ENSO	1.87	2.28	4.22	0.0011
	ENSO+AMO	1.89	2.38	4.51	0.0046

Table 5.1: Properties of the posterior densities of the ECS for different model configurations. The 5th and 95th percentiles of the posterior distributions form 90% credible intervals. The mode is the peak of the density function, i.e., the most probable value of the parameter. $P(\text{ECS} > 10)$ is the probability that the ECS exceeds 10°C.

increases w_{aero} slightly across both temperature datasets.

The scale factor for volcanic aerosols, w_{volc}, has posterior distributions focused on much lower values than the prior. In Figure 5.3 both the posterior distributions and the prior is visualized. In the same figure the posteriors of the effective diffusivity κ are shown. They are focused around 0.3-0.5 $\text{cm}^2\ \text{s}^{-1}$, i.e., in the low end of the prior. Including ICV in the model yields slightly higher values of κ. Again, higher diffusivity means that the surface box temperature reacts slower to an increase in external forcing. A pattern can be recognized where introducing ENSO in the model leads to higher diffusivity and a lower weight on volcanic aerosols. A higher κ for a given set of w_{volc}, h and ECS means that volcanic eruptions are less noticeable in the surface box temperature, while the OHC signal increases. Since the OHC data used here is pentadal, the short-term impacts that volcanic eruptions bring are suppressed. This is probably a reason for that the posterior distribution of the weight is so much lower than its prior. Another reason might be the lamentable lack of data after September 2012.

The aerosol path weights have in most cases posterior distributions quite similar to their prior, $\mathcal{N}(1, 0.1^2)$. The piecewise linear part of the weight function is shown in the bottom right image in Figure 5.3. Again, this function is multiplied by w_{aero} to get the full aerosol weight function. Recall that a high weight means a bigger contribution of aerosols to the radiative forcing, i.e., a lower value of RF and a lower temperature in the following years. Therefore one would expect that trends for the aerosol path would be opposite the trends for the GMST. This holds primarily for the HadCRUT data: Decreasing aerosol weights over 1900-1940, and increasing weights from 2000 to 2013 is consistent with this way of reasoning. In the results for the NOAA data those two trends are more subtle, but the high value of w_{1980} helps explaining both the 1945-1975 cooling and the 1975-2000 warming trends.

Results obtained when evaluating the models with parameters set to the modes of their posterior distributions can be found in Table 5.2. It is clear that including ENSO improves the temperature fit; it removes 26% of the temperature mean ab-

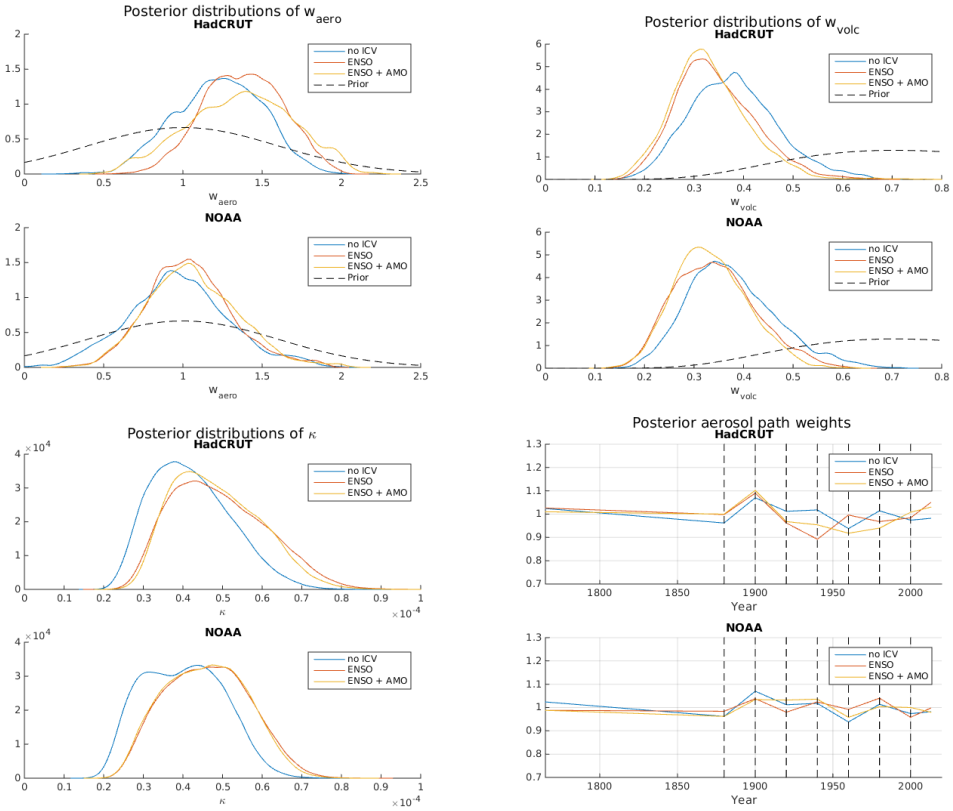

Figure 5.3: Posterior distributions of w_{aero} (top left), w_{volc} (top right) and κ (bottom left) for different model configurations. The bottom right image shows the aerosol path weight functions using the posterior mode of each weight.

solute error (MAE) and 38% of the mean squared error (MSE) for the HadCRUT temperature data. For the NOAA temperature data the corresponding numbers are 22% and 29%. The OHC errors however are more difficult to interpret: For HadCRUT they do not change very much, but for NOAA they are significantly higher when ENSO is included. When adding AMO to the model, temperature errors do not decrease. This is a notable result which will be discussed in chapter 6.

Temp. dataset	Model	OHC		Temperature	
		MAE	MSE	MAE	MSE
HadCRUT	no ICV	0.7820	1.0461	0.0795	0.0093
	ENSO	0.7662	1.0683	0.0585	0.0058
	ENSO+AMO	0.9386	1.4337	0.0606	0.0060
NOAA	no ICV	0.7820	1.0461	0.0720	0.0076
	ENSO	0.8502	1.2102	0.0561	0.0054
	ENSO+AMO	0.7949	1.0906	0.0559	0.0053

Table 5.2: Evaluation results. MAE indicates mean absolute error, MSE mean squared error.

In Figure 5.4 the similarities and differences between the observed and the modeled temperature are illustrated. The model used in this case was ENSO+AMO using HadCRUT temperature data. The observed data is plotted along with each year's 90% interval for the modeled temperature. We see that the model captures the 21st century hiatus fairly well. However, we know from Table 5.2 that the errors are even smaller when the AMO is not considered, and indeed the hiatus is modeled quite well when that is the case as well. A corresponding image to Figure 5.4 but without AMO in the model is shown in appendix B, Figure B.2. Also shown in the very same appendix, Figure B.3, is a corresponding graph but for the estimated and observed OHC, instead of temperature.

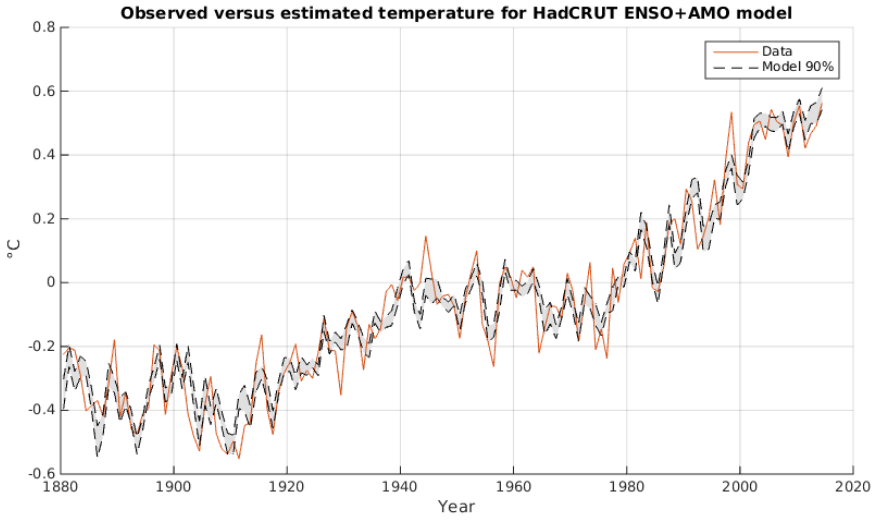

Figure 5.4: Observed and modeled temperature, for the HadCRUT temperature data and ENSO+AMO model. The model intervals are constructed by taking the 5th and 95th percentiles of each year's temperature estimate.

5.1 AMO data from HadSST

The parameter that is affected the most from changing the source of AMO data is naturally β_{AMO}, the AMO regression coefficient. A comparison between the posterior distributions for β_{AMO} using different AMO data is given in the left image of Figure 5.5. We see that for both temperature datasets, using the HadSST AMO data nudges the posterior distributions of β_{AMO} to the right. The change is not very large and the most important facts still stand: For HadCRUT temperature data, β_{AMO} is still significant at the $\alpha = 0.05$ level, and for NOAA temperature data β_{AMO} is still not significant at all. A comparison of the ECS for the ENSO+AMO model with different AMO data sources can be seen in the right image of Figure 5.5. Here the 90% intervals of the ECS are (2.13, 8.37) for HadCRUT and (1.84, 4.28) for the NOAA temperature data. Comparing these to the intervals presented in Table 5.1, as well as inspecting the right image in Figure 5.5, reveals that the

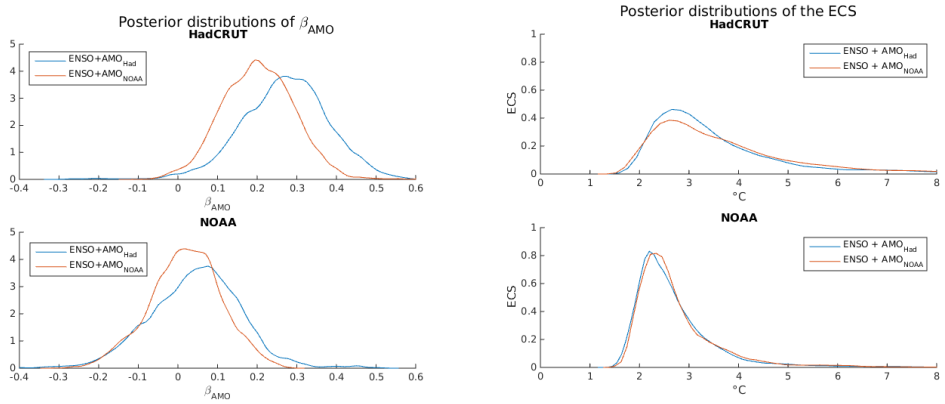

Figure 5.5: Posterior distributions of β_{AMO} (left) and ECS (right) for different AMO data sources.

ECS estimates are slightly affected when the AMO data source is changed. For both datasets, the right tails of the posterior distributions become less pronounced. The probability of an ECS greater than 10°C is 3.6% for HadCRUT temperature data, and <0.01% for NOAA temperature data. Still, at least for the HadCRUT data, the right tail of the posterior distribution of the ECS becomes heavier when the AMO is included compared to when it is not. No other parameters than β_{AMO} and the ECS are significantly affected when changing the AMO data source, so no further plots depicting posterior distributions will be shown here.

5.2 Fixed aerosol path

To analyze the consequences of the flexible aerosol path, simulations are also run with a fixed aerosol path for comparison. First of all, the posteriors of the ECS become narrower, which is expected. This can be seen by comparing the left image in Figure 5.6 and Figure 5.2. A fixed aerosol path closes some possibilities and makes the whole model less flexible, which should narrow the posteriors of many parameters. In Table 5.3 some properties of the posterior distributions of the ECS are shown. This table can be compared to Table 5.1, where the corresponding numbers are presented for the variable aerosol path. The posterior mode is higher when the aerosol path is held fixed for all models except the HadCRUT ENSO, where it is almost identical (2.99 versus 3.00). This is especially apparent for the models using the NOAA temperature dataset, where the ECS mode is approx. 0.3-0.4°C higher when the aerosol path is held fixed. Note that including AMO in the model does not increase the probability of high values of ECS in the same way as for the flexible aerosol path. Instead $P(\text{ECS} > 4.5)$, the probability of an ECS value greater than 4.5°C, decreases when AMO is added and the HadCRUT temperature data is used. Regarding other parameters, the right image in Figure 5.6 shows that the w_{aero} posteriors are much more similar over datasets. The posteriors using the HadCRUT data are lower, and the NOAA data higher, than when the aerosol path is allowed to vary. In other words, the differences found by using different temperature datasets seem to be smaller when the aerosol path is fixed. The ENSO parameters β_{ENSO}

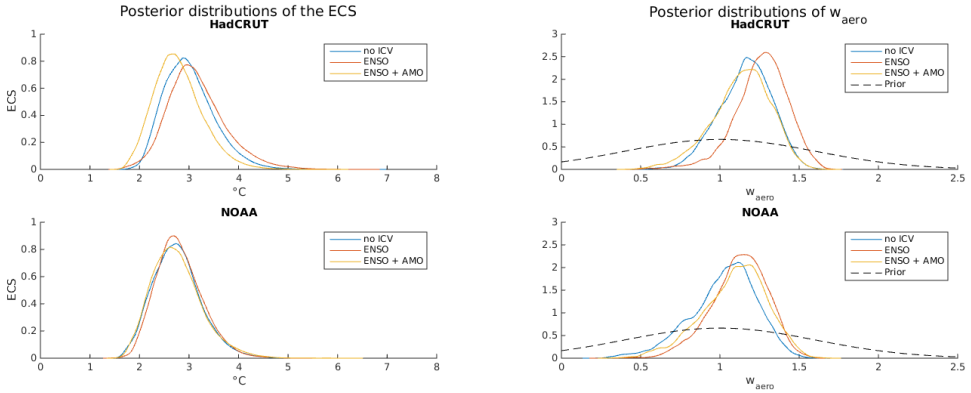

Figure 5.6: Posterior distributions of the ECS (left) and w_{aero} (right), when the aerosol path is held fixed.

Temp. dataset	Model	5th perc.	Mode	95th perc.	$P(\text{ECS} > 4.5)$
HadCRUT	no ICV	2.27	2.88	3.94	0.0091
	ENSO	2.31	2.99	4.23	0.0254
	ENSO+AMO	2.06	2.65	3.68	0.0034
NOAA	no ICV	2.02	2.74	3.63	0.0025
	ENSO	2.11	2.72	3.65	0.0028
	ENSO+AMO	2.02	2.64	3.70	0.0043

Table 5.3: Properties of the posterior densities of the ECS for different model configurations, when the aerosol path is held fixed. Compare to table 5.1 for the flexible aerosol path. The 5th and 95th percentiles of the posterior distributions form 90% credible intervals. The mode is the peak of the density function. $P(\text{ECS} > 10)$ has been excluded since it is 0 for all models, and replaced by $P(\text{ECS} > 4.5)$.

do practically not change at all. The AMO parameters β_{AMO} become slightly lower but the facts of importance still hold; For HadCRUT temperature data β_{AMO} is significant at the $\alpha = 0.05$ level, for NOAA temperature data it is not significant at all. In accordance with earlier discussions regarding the strong connection between the ECS or λ and the weight of anthropogenic aerosols, w_{aero}, the latter's posteriors become significantly narrower when the aerosol path is held fixed, just as is the case for the ECS.

Switching the AMO data source to the HadSST dataset yields 90% posterior ECS intervals of (2.03, 3.66) for HadCRUT data and (1.95, 3.66) for NOAA data. Comparing these intervals to the ones presented in Table 5.3 using the AMO index calculated from NOAA data, shows that the differences are very small. This is consistent with the variable aerosol path case, as presented in section 5.1. The posterior distributions of the regression coefficient β_{AMO} are barely changed at all. This, and some other posterior distributions for parameters using the fixed aerosol path can be seen in appendix B.1. A table corresponding to Table 5.2 but for the fixed aerosol path, containing model errors, is given in appendix A.2. Just as for the flexible

aerosol path, ENSO lowers the temperature errors by a considerable amount. The errors do not decrease when AMO is included, which is also consistent with the flexible aerosol path results.

6
Discussion

The posterior ECS intervals presented in this study for the variable aerosol path model are wide, at least for the HadCRUT data, compared to other recent estimates: IPCC's AR5 mentions (1.5, 4.5) as a 90% interval (Collins et al., 2013), and more recently Johansson et al. (2015) estimated the same interval to be roughly (2.0, 3.2), although they state that their width might be on the low side. When Johansson et al. (2015) do not include ENSO in their analysis, the interval shifts to the right and widens to (2.1, 3.8). This is not at all the case here: For the HadCRUT temperature data the ECS estimates increase when ENSO is included, and for the NOAA temperature data they do not change. The fixed aerosol path results agree overall to a much wider extent with previous literature's results, which is expected since almost all earlier studies consider it fixed.

Another interesting result is that including the AMO in the regression on temperature only reduces the estimated ECS slightly. Earlier papers have concluded AMO can be credited for a large part of the late 20th-century warming trend. Specifically J. Zhou and Tung (2013) find that including AMO reduces the warming trend by a factor of at least two, and both Chylek, Klett, et al. (2014) and Wu et al. (2011) suggest that up to one third of late 20th-century warming can be credited to the AMO. Although none of the mentioned papers discuss the actual effect on the ECS, it is reasonable to believe that these results would imply a lower ECS estimate when the AMO is included in the analysis. In this study this is true for HadCRUT temperature data, as the ECS in the ENSO+AMO model has a lower posterior mode than in the ENSO model, both for flexible and fixed aerosol paths, but the change is small. For the NOAA temperature data the AMO does not have a statistically significant impact on the GMST, so including AMO does not change the ECS estimates. It should be noted that the study conducted by Skeie et al. (2014) is similar in approach to the one presented here. They find that including long-term variability leads to two changes in the estimated ECS: The mode is marginally lowered, and the uncertainty is substantially greater than when no long-term variability is considered. The increase in uncertainty can be recognized in this study's results for the flexible aerosol path, but curiously not for the fixed aerosol path.

Overall, variations in results over temperature datasets are massive. This reveals a problematic sensitivity to experimental design. This result is not new; Libardoni and Forest (2011) analyze the ECS using several different datasets, and they find that the ECS estimate using HadCRUT data is slightly larger and with a heavier right tail than the estimate using NOAA data. They find 90% intervals for the ECS

to be (1.9, 5.1) for HadCRUT3 and (1.8, 4.7) for NOAA data. Their difference is not as large as that found here, but they use older versions of both the HadCRUT and NOAA datasets. As seen at the start of this report in Figure 1.1, the difference between the temperature datasets is seemingly not that large. However, their uncertainties differ substantially, as seen in Figure B.1. This is possibly a reason for the large differences in results between the two temperature datasets. Investigating this could be interesting for future research.

The uncertainty in the historical RF contribution of anthropogenic aerosols has been overlooked in many earlier studies. The flexible aerosol path presented here takes into consideration that not only the scale factor of aerosols, but the actual aerosol path as well, is uncertain. The result is a much higher probability of a large ECS. For the fixed aerosol path the estimated probability of the ECS being greater than 10°C is zero for all models. When the aerosol path is flexible the probability rises to as much as 2% for the ENSO model, and 6% for the ENSO+AMO model, with HadCRUT temperature data. As a comparison, Aldrin et al. (2012) report a corresponding probability of 0.1% for their model, which has a fixed aerosol path and considers ENSO but no interdecadal variability. Skeie et al. (2014) report a 0.1% probability of the ECS being greater than 4.5°C when they do not consider long-term variability, which rises to 1.4% when they do. The results for the fixed aerosol path presented in section 5.2, and specifically Table 5.3, do not show this trend, as including AMO actually lowers the probability of high ECS for HadCRUT temperature data, and only increases it marginally for NOAA data. Again, for the flexible path these values are much higher overall.

It should be noted that the choice of priors for the aerosol path weights could have a large impact on the results. The priors chosen here are all normally distributed with standard deviation 0.1. It would be interesting to investigate how the results change when other priors are used. One could possibly consider the prior standard deviations to be decreasing with time.

7
Conclusions

This study has examined the impact of aerosol path flexibility and internal climate variability on the global mean surface temperature and the equilibrium climate sensitivity (ECS). The ECS is defined as the equilibrium change in global mean surface temperature that a doubling of the pre-industrial atmospheric CO_2 concentration would bring. The aerosol path flexibility substantially increases the probability of very high values of the ECS, but marginally decreases the most probable value. The 90% intervals for the ECS using HadCRUT temperature data and both short- and long-term internal variability are (2.07, 11.58) for the flexible aerosol path and (2.06, 3.68) for the fixed aerosol path. Using different datasets for the global mean surface temperature changes the results considerably for the flexible aerosol path: The corresponding intervals using temperature data from NOAA are (1.89, 4.51) and (2.02, 3.70).

The impact of interdecadal internal variability on the global mean surface temperature is frequently debated. The results presented here does not show consensus between different datasets on this. Such internal variability in the form of the AMO index is statistically significant when using the HadCRUT temperature dataset, but not for the NOAA data. In the cases where the AMO has a statistically significant impact on the global mean surface temperature, the estimated equilibrium climate sensitivity is slightly lowered. The estimated temperature does not come closer to observed data with the introduction of AMO to the model. This means that interdecadal internal climate variability might have a smaller effect on the global mean surface temperature than some earlier work suggests. It also indicates that observed historical multidecadal temperature oscillations might be better explained by changes in external forcing than by the AMO.

The differences between temperature datasets might be partly due to large discrepancies in their observational uncertainties, but investigating this could be an intriguing question for future work. Further exploring the effects of historical uncertainty of the aerosol path is another possible research direction. Investigating the consequences of the choice of priors associated with the aerosol path, or search for other ways of expressing the historical uncertainty, might be interesting areas for future research.

Bibliography

Aldrin, Magne, Marit Holden, Peter Guttorp, Ragnhild B. Skeie, Gunnar Myhre, and Terje K. Berntsen (2012). "Bayesian estimation of climate sensitivity based on a simple climate model fitted to observations of hemispheric temperatures and global ocean heat content". In: *Environmetrics* 23 (3), pp. 253–271. DOI: 10.1002/env.2140.

Bindoff, N. L. et al. (2013). "Detection and Attribution of Climate Change: from Global to Regional". In: *Climate Change 2013: The Physical Science Basis. Contribution of Working Group I to the Fifth Assessment Report of the Intergovernmental Panel on Climate Change*. Ed. by T. F. Stocker et al. Cambridge, United Kingdom and New York, NY, USA: Cambridge University Press. Chap. 10, pp. 867–952. ISBN: 978-1-107-66182-0. DOI: 10.1017/CBO9781107415324.022. URL: www.climatechange2013.org.

Booth, Ben B. B., Nick J. Dunstone, Paul R. Halloran, Timothy Andrews, and Nicolas Bellouin (2012). "Aerosols implicated as a prime driver of twentieth-century North Atlantic climate variability". In: *Nature* 484 (7393), pp. 228–232. DOI: 10.1038/nature10946.

Boucher, O. et al. (2013). "Clouds and Aerosols". In: *Climate Change 2013: The Physical Science Basis. Contribution of Working Group I to the Fifth Assessment Report of the Intergovernmental Panel on Climate Change*. Ed. by T. F. Stocker et al. Cambridge, United Kingdom and New York, NY, USA: Cambridge University Press. Chap. 7, pp. 571–658. ISBN: 978-1-107-66182-0. DOI: 10.1017/CBO9781107415324.016. URL: www.climatechange2013.org.

Chen, Xianyao and Ka-Kit Tung (2014). "Varying planetary heat sink led to global-warming slowdown and acceleration". In: *Science* 345 (6199), pp. 897–903. DOI: 10.1126/science.1254937.

Chylek, Petr, Chris Folland, Leela Frankcombe, Henk Dijkstra, Glen Lesins, and Manvendra Dubey (2012). "Greenland ice core evidence for spatial and temporal variability of the Atlantic Multidecadal Oscillation". In: *Geophysical Research Letters* 39 (9). DOI: 10.1029/2012GL051241.

Chylek, Petr, James D. Klett, Glen Lesins, Manvendra K. Dubey, and Nicolas Hengartner (2014). "The Atlantic Multidecadal Oscillation as a dominant factor of oceanic influence on climate". In: *Geophysical Research Letters* 41 (5), pp. 1689–1697. DOI: 10.1002/2014GL059274.

Climate Prediction Center (2012). *Frequently asked questions about El Niño and La Niña*. NOAA. URL: http://www.cpc.noaa.gov/products/analysis_monitoring/ensostuff/ensofaq.shtml#HOWOFTEN (visited on Apr. 20, 2015).

Collins, M. et al. (2013). "Long-term Climate Change: Projections, Commitments and Irreversibility". In: *Climate Change 2013: The Physical Science Basis. Contribution of Working Group I to the Fifth Assessment Report of the Intergovernmental Panel on Climate Change*. Ed. by T. F. Stocker et al. Cambridge, United Kingdom and New York, NY, USA: Cambridge University Press. Chap. 12, pp. 1029–1136. ISBN: 978-1-107-66182-0. DOI: 10.1017/CBO9781107415324.024. URL: www.climatechange2013.org.

Cowtan, Kevin, Peter Jacobs, and Robert G. Way (2015). "Response to Gleisner et al (2015)". Unpublished. URL: http://www-users.york.ac.uk/~kdc3/papers/coverage2013/gleisner-response.pdf.

Cowtan, Kevin and Robert G. Way (2014). "Coverage bias in the HadCRUT4 temperature series and its impact on recent temperature trends". In: *Quarterly Journal of the Royal Meteorological Society* 140 (683), pp. 1935–1944. DOI: 10.1002/qj.2297.

Cubasch, U. et al. (2001). "Projections of Future Climate Change". In: *Climate Change 2001: The Scientific Basis. Contribution of Working Group I to the Third Assessment Report of the Intergovernmental Panel on Climate Change*. Ed. by J. T. Houghton, Y. Ding, D. J. Griggs, M. Noguer, P. J. van der Linden, X. Dai, K. Maskell, and C. A. Johnson. Cambridge, United Kingdom and New York, NY, USA: Cambridge University Press. Chap. 9, pp. 525–582. ISBN: 0521-80767-0. URL: http://www.grida.no/climate/ipcc_tar/wg1/index.htm.

Delworth, Tom L. and Michael E. Mann (2000). "Observed and simulated multidecadal variability in the Northern Hemisphere". In: *Climate Dynamics* 16 (9), pp. 661–676. DOI: 10.1007/s003820000075.

Dlugokencky, Ed and Pieter Tans (2015). *Trends in Atmospheric Carbon Dioxide*. NOAA/ESRL. URL: www.esrl.noaa.gov/gmd/ccgg/trends/ (visited on June 9, 2015).

Douville, Hervé, Aurore Voldoire, and Olivier Geoffroy (2015). "The recent global warming hiatus: What is the role of Pacific variability?" In: *Geophysical Research Letters* 42 (3), pp. 880–888. DOI: 10.1002/2014GL062775.

Dunne, John P. (2014). *Earth System Models*. NOAA. URL: http://www.gfdl.noaa.gov/earth-system-model (visited on Apr. 11, 2015).

Edwards, Paul N. (2001). "A brief history of atmospheric general circulation modeling". In: *Circulation Model Development*. Ed. by David A. Randall. Vol. 70. International Geophysics. Academic Press, pp. 67–90. DOI: http://dx.doi.org/10.1016/S0074-6142(00)80050-9.

England, Matthew H. et al. (2014). "Recent intensification of wind-driven circulation in the Pacific and the ongoing warming hiatus". In: *Nature Climate Change* 4 (3), pp. 222–227. DOI: 10.1038/nclimate2106.

Flato, G. et al. (2013). "Evaluation of Climate Models". In: *Climate Change 2013: The Physical Science Basis. Contribution of Working Group I to the Fifth Assessment Report of the Intergovernmental Panel on Climate Change*. Ed. by T. F. Stocker et al. Cambridge, United Kingdom and New York, NY, USA: Cambridge University Press. Chap. 9, pp. 741–882. ISBN: 978-1-107-66182-0. DOI: 10.1017/CBO9781107415324.020. URL: www.climatechange2013.org.

Foster, Grant and Stefan Rahmstorf (2011). "Global temperature evolution 1979–2010". In: *Environmental Research Letters* 6 (4). DOI: 10.1088/1748-9326/6/4/044022.

Fröhlich, Claus (2000). "Observations of Irradiance Variations". In: *Space Science Reviews* 94 (1-2), pp. 15–24. DOI: 10.1023/A:1026765712084. Data available at http://climexp.knmi.nl/data/itsi.dat (visited on Jan. 22, 2015).

Fyfe, John C., Nathan P. Gillett, and Francis W. Zwiers (2013). "Overestimated global warming over the past 20 years". In: *Nature Climate Change* 3 (9), pp. 767–769. DOI: 10.1038/nclimate1972.

Geoffroy, Olivier, David Saint-Martin, Dirk J.L. Olivié, Aurore Voldoire, Gilles Bellon, and Sophie Tytéca (2013). "Transient climate response in a two-layer energy-balance model. Part I: Analytical solution and parameter calibration using CMIP5 AOGCM experiments". In: *Journal of Climate* 26 (6), pp. 1841–1857. DOI: 10.1175/JCLI-D-12-00195.1.

Gleisner, Hans, Peter Thejll, Bo Christiansen, and Johannes K. Nielsen (2015). "Recent global warming hiatus dominated by low-latitude temperature trends in surface and troposphere data". In: *Geophysical Research Letters* 42 (2), pp. 510–517. DOI: 10.1002/2014GL062596.

Goddard Institute for Space Studies (2015). *Forcings in GISS Climate Model. Stratospheric Aerosol Optical Thickness*. NASA. URL: http://data.giss.nasa.gov/modelforce/strataer/ (visited on Jan. 22, 2015).

Gray, Stephen T., Lisa J. Graumlich, Julio L. Betancourt, and Gregory T. Pederson (2004). "A tree-ring based reconstruction of the Atlantic Multidecadal Oscillation since 1567 A.D." In: *Geophysical Research Letters* 31 (12). DOI: 10.1029/2004GL019932.

Johansson, Daniel J.A. (2011). "Temperature stabilization, ocean heat uptake and radiative forcing overshoot profiles". In: *Climatic Change* 108.1-2, pp. 107–134. DOI: 10.1007/s10584-010-9969-4.

Johansson, Daniel J.A., Brian C. O'Neill, Claudia Tebaldi, and Olle Häggström (2015). "Equilibrium climate sensitivity in light of observations over the warming hiatus". In: *Nature Climate Change* 5 (5), pp. 449–453. DOI: 10.1038/nclimate2573.

Kaufmann, Robert K., Heikki Kauppi, Michael L. Mann, and James H. Stock (2011). "Reconciling anthropogenic climate change with observed temperature 1998–2008". In: *Proceedings of the National Academy of Sciences* 108 (29), pp. 11790–11793. DOI: 10.1073/pnas.1102467108.

Knudsen, Mads F., Bo H. Jacobsen, Marit-Solveig Seidenkrantz, and Jesper Olsen (2014). "Evidence for external forcing of the Atlantic Multidecadal Oscillation since termination of the Little Ice Age". In: *Nature Communications* 5 (3323). DOI: 10.1038/ncomms4323.

Kosaka, Yu and Shang-Ping Xie (2013). "Recent global-warming hiatus tied to equatorial Pacific surface cooling". In: *Nature* 501 (7467), pp. 403–407. DOI: 10.1038/nature12534.

Kriegler, Elmar (2005). "Imprecise probability analysis for integrated assessment of climate change". PhD thesis. University of Potsdam.

Libardoni, Alex G. and Chris E. Forest (2011). "Sensitivity of distributions of climate system properties to the surface temperature dataset". In: *Geophysical Research Letters* 38 (22). DOI: 10.1029/2011GL049431.

Link, William A. and Mitchell J. Eaton (2012). "On thinning of chains in MCMC". In: *Methods in Ecology and Evolution* 3 (1), pp. 112–115. DOI: 10.1111/j.2041-210X.2011.00131.x.

MacEachern, Steve N. and L. Mark Berliner (1994). "Subsampling the Gibbs Sampler". In: *The American Statistician* 48 (3), pp. 188–190. DOI: 10.1080/00031305.1994.10476054.

Manabe, Syukuro and Kirk Bryan (1969). "Climate calculations with a combined ocean-atmosphere model". In: *Journal of the Atmospheric Sciences* 26 (4), pp. 786–789.

Mann, Michael E. (2004). "On smoothing potentially non-stationary climate time series". In: *Geophysical Research Letters* 31 (7). DOI: 10.1029/2004GL019569.

Mantua, Nathan J. (2003). "Pacific–Decadal Oscillation". In: *Encyclopedia of Global Environmental Change, Volume 1, The Earth System: Physical and Chemical Dimensions of Global Environmental Change*. Ed. by Michael C. MacCracken and John S. Perry. Chichester, UK: Wiley, pp. 592–594. ISBN: 978-0-470-85360-3.

Meinshausen, Malte (2011). *RCP Concentration Calculations and Data*. Potsdam Institute for Climate Impact Research. URL: http://www.pik-potsdam.de/~mmalte/rcps/ (visited on Jan. 22, 2015).

Meinshausen, Malte et al. (2011). "The RCP greenhouse gas concentrations and their extensions from 1765 to 2300". In: *Climatic Change* 109 (1-2), pp. 213–241. DOI: 10.1007/s10584-011-0156-z.

Met Office Hadley Centre (2015). *Met Office Hadley Centre observations datasets. HadCRUT4 Data: download*. URL: http://www.metoffice.gov.uk/hadobs/hadcrut4/data/current/download.html (visited on Feb. 20, 2015).

Metropolis, Nicholas, Arianna W. Rosenbluth, Marshall N. Rosenbluth, Augusta H. Teller, and Edward Teller (1953). "Equation of State Calculations by Fast Computing Machines". In: *The Journal of Chemical Physics* 21 (6), pp. 1087–1092. DOI: 10.1063/1.1699114.

Morice, Colin P., John J. Kennedy, Nick A. Rayner, and Phil D. Jones (2012). "Quantifying uncertainties in global and regional temperature change using an ensemble of observational estimates: The HadCRUT4 data set". In: *Journal of Geophysical Research: Atmospheres* 117 (D8), pp. 1–22. DOI: 10.1029/2011JD017187.

Myhre, G. et al. (2013). "Anthropogenic and Natural Radiative Forcing". In: *Climate Change 2013: The Physical Science Basis. Contribution of Working Group I to the Fifth Assessment Report of the Intergovernmental Panel on Climate Change*. Ed. by T. F. Stocker et al. Cambridge, United Kingdom and New York, NY, USA: Cambridge University Press. Chap. 8, pp. 659–740. ISBN: 978-1-107-66182-0. DOI: 10.1017/CBO9781107415324.018. URL: www.climatechange2013.org.

National Climatic Data Center (2015a). *ENSO Technical Discussion*. NOAA. URL: https://www.ncdc.noaa.gov/teleconnections/enso/enso-tech.php (visited on Apr. 20, 2015).

— (2015b). *Index of /pub/data/mlost/operational/products*. NOAA. URL: http://www1.ncdc.noaa.gov/pub/data/mlost/operational/products/ (visited on Feb. 2, 2015).

National Oceanographic Data Center (2015). *Basin time series of heat content*. NOAA. URL: http://www.nodc.noaa.gov/OC5/3M_HEAT_CONTENT/basin_data.html (visited on Feb. 10, 2015).

van Oldenborgh, Geert Jan (2015). *KNMI Climate Explorer*. Royal Netherlands Meteorological Institute. URL: http://climexp.knmi.nl/selectindex.cgi?id=someone@somewhere (visited on Apr. 3, 2015).

Otterå, Odd Helge, Mats Bentsen, Helge Drange, and Lingling Suo (2010). "External forcing as a metronome for Atlantic multidecadal variability". In: *Nature Geoscience* 3 (10), pp. 688–694. DOI: 10.1038/ngeo955.

Rahmstorf, Stefan (2008). "Anthropogenic climate change: Revisiting the facts". In: *Global Warming: Looking Beyond Kyoto*. Ed. by Ernesto Zedillo. Washington, D.C., USA: Brookings Institution Press. Chap. 3, pp. 34–53. ISBN: 0-8157-9714-1.

Roberts, Craig D., Matthew D. Palmer, Doug McNeall, and Mat Collins (2015). "Quantifying the likelihood of a continued hiatus in global warming". In: *Nature Climate Change* 5 (4), pp. 337–342. DOI: 10.1038/nclimate2531.

Roberts, Gareth O., Andrew Gelman, and Walter R. Gilks (1997). "Weak convergence and optimal scaling of random walk Metropolis algorithms". In: *The Annals of Applied Probability* 7 (1), pp. 110–120. DOI: 10.1214/aoap/1034625254.

Roemmich, Dean, John Church, John Gilson, Didier Monselesan, Philip Sutton, and Susan Wijffels (2015). "Unabated planetary warming and its ocean structure since 2006". In: *Nature Climate Change* 5 (3), pp. 240–245. DOI: 10.1038/nclimate2513.

Rogers, Jeffrey C. and Jill S.M. Coleman (2003). "Interactions between the Atlantic Multidecadal Oscillation, El Nino/La Nina, and the PNA in winter Mississippi valley stream flow". In: *Geophysical Research Letters* 30 (10). DOI: 10.1029/2003GL017216.

Sherwood, Steven C., Sandrine Bony, and Jean-Louis Dufresne (2014). "Spread in model climate sensitivity traced to atmospheric convective mixing". In: *Nature* 505 (7481), pp. 37–42. DOI: 10.1038/nature12829.

Skeie, Ragnhild B., Terje K. Berntsen, Magne Aldrin, Marit Holden, and Gunnar Myhre (2014). "A lower and more constrained estimate of climate sensitivity using updated observations and detailed radiative forcing time series". In: *Earth System Dynamics* 5 (1), pp. 139–175. DOI: 10.5194/esd-5-139-2014.

Tanaka, Katsumasa, Thomas Raddatz, Brian C. O'Neill, and Christian H. Reick (2009). "Insufficient forcing uncertainty underestimates the risk of high climate sensitivity". In: *Geophysical Research Letters* 36 (16). DOI: 10.1029/2009GL039642.

Titus, James G. and Vijay Narayanan (1996). "The risk of sea level rise". In: *Climatic Change* 33 (2), pp. 151–212. DOI: 10.1007/BF00140246.

Tomassini, Lorenzo, Peter Reichert, Reto Knutti, Thomas F. Stocker, and Mark E. Borsuk (2007). "Robust Bayesian Uncertainty Analysis of Climate System Properties Using Markov Chain Monte Carlo Methods". In: *Journal of Climate* 20 (7), pp. 1239–1254. DOI: 10.1175/JCLI4064.1.

Trenberth, Kevin E. (1997). "The Definition of El Niño". In: *Bulletin of the American Meteorological Society* 78 (12), pp. 2771–2777. DOI: 10.1175/1520-0477(1997)078<2771:TDOENO>2.0.CO;2.

Trenberth, Kevin E., Julie M. Caron, David P. Stepaniak, and Steve Worley (2002). "Evolution of El Niño–Southern Oscillation and global atmospheric surface temperatures". In: *Journal of Geophysical Research: Atmospheres* 107.D8, pp. 5.1–5.17. DOI: 10.1029/2000JD000298.

Trenberth, Kevin E. and John T. Fasullo (2013). "An apparent hiatus in global warming?" In: *Earth's Future* 1 (1), pp. 19–32. DOI: 10.1002/2013EF000165.

Trenberth, Kevin E., P. D. Jones, et al. (2007). "Observations: surface and atmospheric climate change". In: *Climate Change 2007: Working Group I: The Physical Science Basis*. Ed. by S. Solomon, D. Qin, M. Manning, Z. Chen, M. Marquis, K. B. Averyt, M. Tignor, and H. L. Miller. Cambridge, United Kingdom and New York, NY, USA: Cambridge University Press, pp. 235–336. ISBN: 978-0-521-70596-7. URL: https://www.ipcc.ch/publications_and_data/ar4/wg1/en/contents.html.

Trenberth, Kevin E. and Dennis J. Shea (2006). "Atlantic hurricanes and natural variability in 2005". In: *Geophysical Research Letters* 33.12. DOI: 10.1029/2006GL026894.

Tung, Ka-Kit and Jiansong Zhou (2013). "Using data to attribute episodes of warming and cooling in instrumental records". In: *Proceedings of the National Academy of Sciences* 110.6, pp. 2058–2063. DOI: 10.1073/pnas.1212471110.

Wang, Chunzai and Liping Zhang (2013). "Multidecadal ocean temperature and salinity variability in the Tropical North Atlantic: linking with the AMO, AMOC, and subtropical Cell". In: *Journal of Climate* 26 (16), pp. 6137–6162. DOI: 10.1175/JCLI-D-12-00721.1.

Wang, Tao, Odd Helge Otterå, Yongqi Gao, and Huijun Wang (2012). "The response of the North Pacific Decadal Variability to strong tropical volcanic eruptions". In: *Climate Dynamics* 39 (12), pp. 2917–2936. DOI: 10.1007/s00382-012-1373-5.

Watanabe, Masahiro, Hideo Shiogama, Hiroaki Tatebe, Michiya Hayashi, Masayoshi Ishii, and Masahide Kimoto (2014). "Contribution of natural decadal variability to global warming acceleration and hiatus". In: *Nature Climate Change* 4 (10), pp. 893–897. DOI: 10.1038/nclimate2355.

Wigley, Tom M.L. and Michael E. Schlesinger (1985). "Analytical solution for the effect of increasing CO2 on global mean temperature". In: *Nature* 315 (6021), pp. 649–652. DOI: 10.1038/315649a0.

Wilcox, Laura J., Eleanor J. Highwood, and Nick J. Dunstone (2013). "The influence of anthropogenic aerosol on multi-decadal variations of historical global climate". In: *Environmental Research Letters* 8 (2). DOI: 10.1088/1748-9326/8/2/024033.

Wu, Zhaohua, Norden E. Huang, John M. Wallace, Brian V. Smoliak, and Xianyao Chen (2011). "On the time-varying trend in global-mean surface temperature". In: *Climate Dynamics* 37 (3-4), pp. 759–773. DOI: 10.1007/s00382-011-1128-8.

Wyatt, Marcia G., Sergey Kravtsov, and Anastasios A. Tsonis (2012). "Atlantic Multidecadal Oscillation and Northern Hemisphere's climate variability". In: *Climate Dynamics* 38 (5-6), pp. 929–949. DOI: 10.1007/s00382-011-1071-8.

Yao, Shuai-Lei, Gang Huang, Ren-Guang Wu, and Xia Qu (2015). "The global warming hiatus—a natural product of interactions of a secular warming trend and a multi-decadal oscillation". In: *Theoretical and Applied Climatology*, pp. 1–12. DOI: 10.1007/s00704-014-1358-x.

Zhou, Chen, Mark D. Zelinka, Andrew E. Dessler, and Ping Yang (2013). "An analysis of the short-term cloud feedback using MODIS data". In: *Journal of Climate* 26 (13), pp. 4803–4815. DOI: 10.1175/JCLI-D-12-00547.1.

Zhou, Jiansong and Ka-Kit Tung (2013). "Deducing Multidecadal Anthropogenic Global Warming Trends Using Multiple Regression Analysis". In: *Journal of the Atmospheric Sciences* 70 (1), pp. 3–8. DOI: 10.1175/JAS-D-12-0208.1.

A

Tables

A.1 Correlations

	Temp. dataset	
Months	HadCRUT	NOAA
0	0.3844	0.3847
1	0.4119	0.4082
2	0.4229	0.4156
3	0.4197	0.4096
4	0.4100	0.3982
5	0.3979	0.3849
6	0.3860	0.3723
7	0.3777	0.3639
8	0.3728	0.3596
9	0.3716	0.3594
10	0.3733	0.3630
11	0.3747	0.3674

Table A.1: Correlations between the NINO3.4 index and GMST, from HadCRUT and NOAA, for different lags. Two months lag maximizes correlation for both datasets.

A.2 Evaluation results for fixed aerosol path

Temp. dataset	Model	OHC		Temperature	
		MAE	MSE	MAE	MSE
HadCRUT	no ICV	0.7320	0.9286	0.0777	0.0089
	ENSO	0.7806	1.0821	0.0597	0.0060
	ENSO+AMO_{NOAA}	0.7509	1.0108	0.0590	0.0058
	ENSO+AMO_{Had}	0.7777	1.0477	0.0591	0.0059
NOAA	no ICV	0.7638	1.0183	0.0716	0.0074
	ENSO	0.7404	1.0103	0.0552	0.0053
	ENSO+AMO_{NOAA}	0.8894	1.3106	0.0557	0.0053
	ENSO+AMO_{Had}	0.8195	1.1531	0.0555	0.0052

Table A.2: Evaluation results for the fixed aerosol path. MAE indicates mean absolute error, MSE mean squared error.

B

Figures

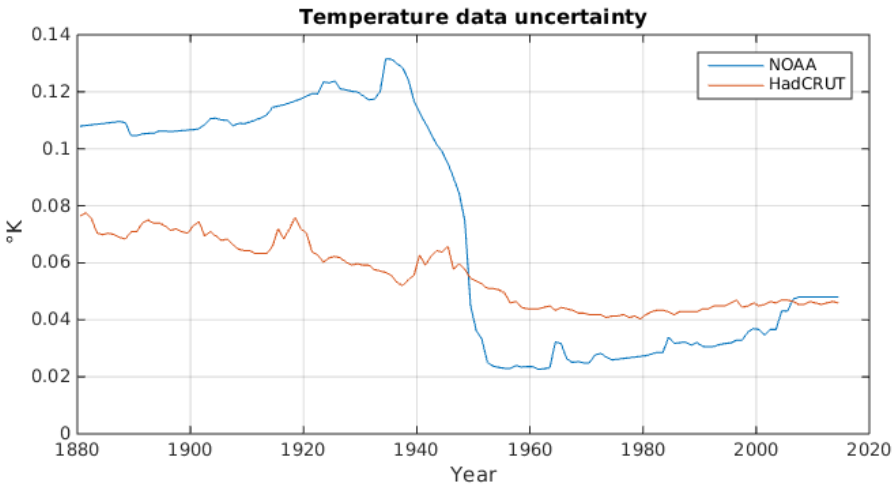

Figure B.1: Temperature data uncertainty for both datasets.

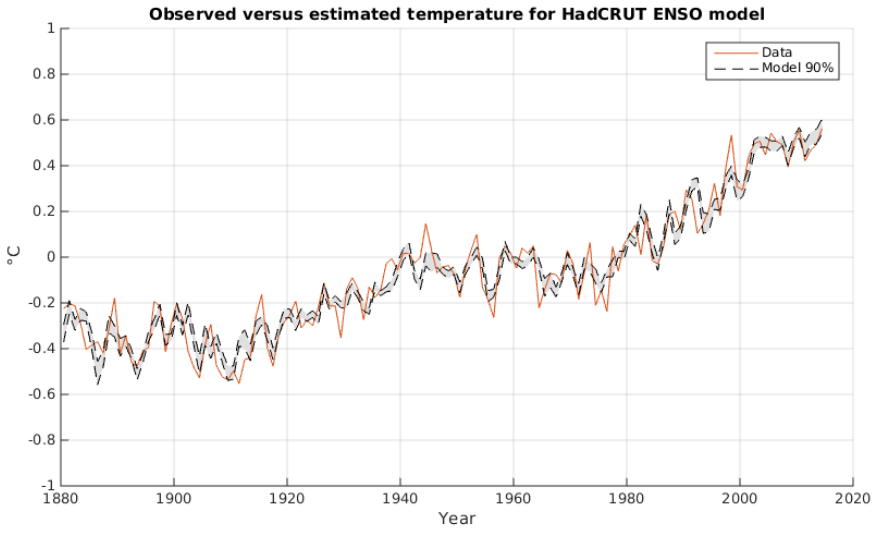

Figure B.2: Observed and modeled temperature, for the HadCRUT temperature data and ENSO model. The model intervals are constructed by taking the 5th and 95th percentiles of each year's temperature estimate.

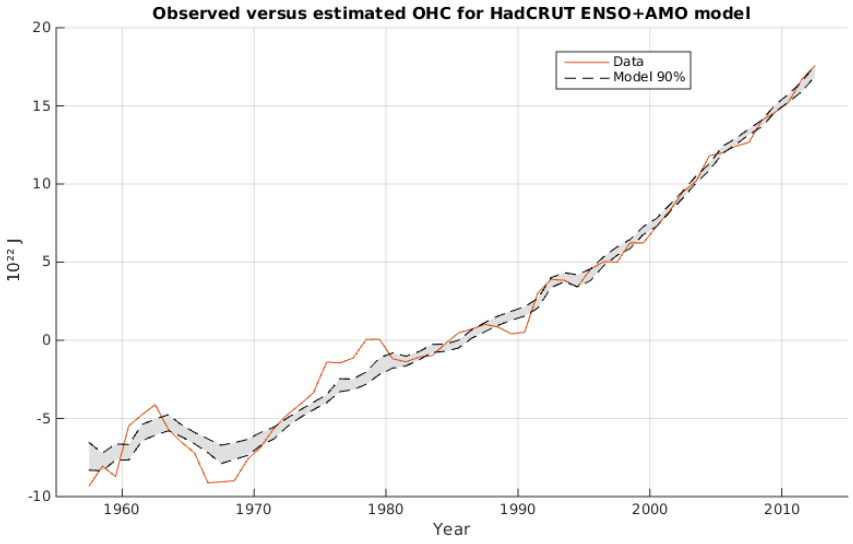

Figure B.3: Observed and modeled OHC, for HadCRUT temperature data and the ENSO+AMO model. The model intervals are constructed by taking the 5th and 95th percentiles of each year's OHC estimate.

B.1 Posterior distributions for fixed aerosol path

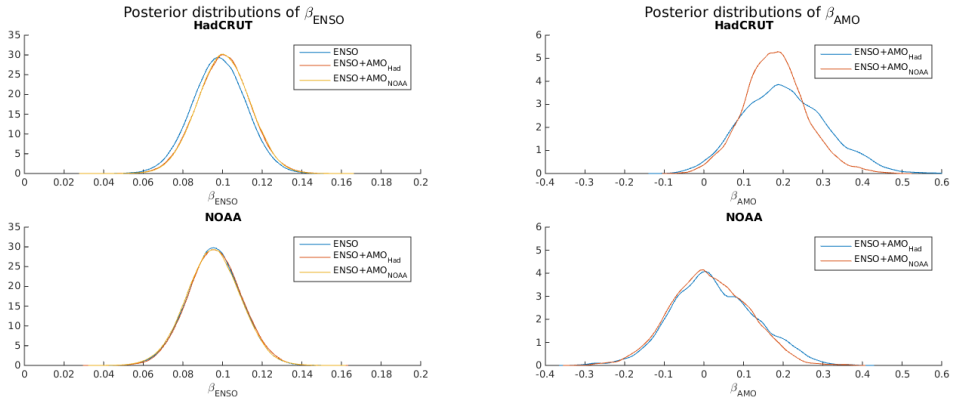

Figure B.4: Posterior distributions of β_{ENSO} (left) and β_{AMO} (right) using the fixed aerosol path.

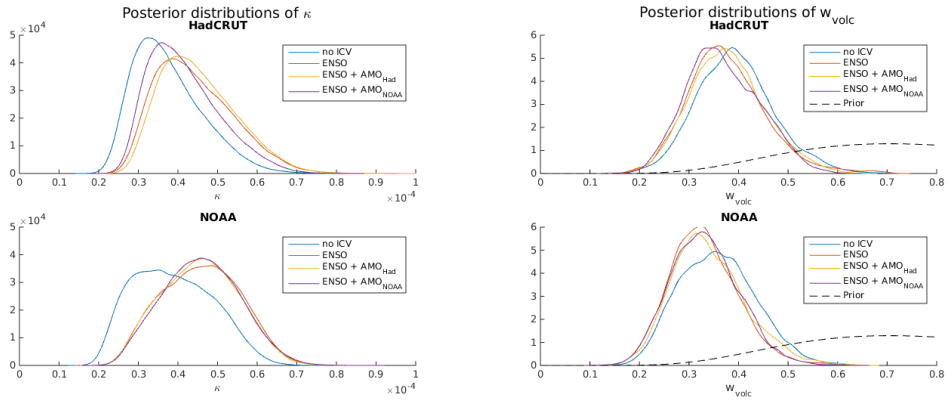

Figure B.5: Posterior distributions of κ (left) and w_{volc} (right) using the fixed aerosol path.